

AperTO - Archivio Istituzionale Open Access dell'Università di Torino

**Probing the evolution of the EAS muon content in the atmosphere with KASCADE-Grande**

**This is a pre print version of the following article:**

*Original Citation:*

*Availability:*

This version is available <http://hdl.handle.net/2318/1653092> since 2017-11-25T11:33:24Z

*Published version:*

DOI:10.1016/j.astropartphys.2017.07.001

*Terms of use:*

Open Access

Anyone can freely access the full text of works made available as "Open Access". Works made available under a Creative Commons license can be used according to the terms and conditions of said license. Use of all other works requires consent of the right holder (author or publisher) if not exempted from copyright protection by the applicable law.

(Article begins on next page)

# 1 Probing the evolution of the EAS muon content in the atmosphere 2 with KASCADE-Grande

3 W.D. Apel<sup>a</sup>, J.C. Arteaga-Velázquez<sup>b,\*</sup>, K. Bekk<sup>a</sup>, M. Bertaina<sup>c</sup>, J. Blümer<sup>a,d,1</sup>,  
4 H. Bozdog<sup>a</sup>, I.M. Brancus<sup>e</sup>, E. Cantoni<sup>c,f,2</sup>, A. Chiavassa<sup>c</sup>, F. Cossavella<sup>d,3</sup>, K. Daumiller<sup>a</sup>,  
5 V. de Souza<sup>g</sup>, F. Di Pierro<sup>c</sup>, P. Doll<sup>a</sup>, R. Engel<sup>a</sup>, D. Fuhrmann<sup>h,4</sup>, A. Gherghel-Lascu<sup>e</sup>,  
6 H.J. Gils<sup>a</sup>, R. Glasstetter<sup>h</sup>, C. Grupen<sup>i</sup>, A. Haungs<sup>a,\*\*</sup>, D. Heck<sup>a</sup>, J.R. Hörandel<sup>j</sup>,  
7 T. Huege<sup>a</sup>, K.-H. Kampert<sup>h</sup>, D. Kang<sup>d</sup>, H.O. Klages<sup>a</sup>, K. Link<sup>d</sup>, P. Łuczak<sup>k</sup>, H.J. Mathes<sup>a</sup>,  
8 H.J. Mayer<sup>a</sup>, J. Milke<sup>a</sup>, B. Mitrica<sup>e</sup>, C. Morello<sup>f</sup>, J. Oehlschläger<sup>a</sup>, S. Ostapchenko<sup>l</sup>,  
9 T. Pierog<sup>a</sup>, H. Rebel<sup>a</sup>, M. Roth<sup>a</sup>, H. Schieler<sup>a</sup>, S. Schoo<sup>a</sup>, F.G. Schröder<sup>a</sup>, O. Sima<sup>m</sup>,  
10 G. Toma<sup>e</sup>, G.C. Trinchero<sup>f</sup>, H. Ulrich<sup>a</sup>, A. Weindl<sup>a</sup>, J. Wochele<sup>a</sup>, J. Zabierowski<sup>k</sup>

11 <sup>a</sup>*Institut für Kernphysik, KIT - Karlsruher Institut für Technologie, Germany*

12 <sup>b</sup>*Institute of Physics and Mathematics, Universidad Michoacana de San Nicolás de Hidalgo, Morelia,*  
13 *Mexico*

14 <sup>c</sup>*Departmento di Fisica, Università degli Studi di Torino, Italy*

15 <sup>d</sup>*Institut für Experimentelle Kernphysik, KIT - Karlsruher Institut für Technologie, Germany*

16 <sup>e</sup>*Horia Hulubei National Institute of Physics and Nuclear Engineering, Bucharest, Romania*

17 <sup>f</sup>*Osservatorio Astrofisico di Torino, INAF Torino, Italy*

18 <sup>g</sup>*Universidade de São Paulo, Instituto de Física de São Carlos, Brasil*

19 <sup>h</sup>*Fachbereich Physik, Universität Wuppertal, Germany*

20 <sup>i</sup>*Department of Physics, Siegen University, Germany*

21 <sup>j</sup>*Department of Astrophysics, Radboud University Nijmegen, The Netherlands*

22 <sup>k</sup>*National Centre for Nuclear Research, Department of Astrophysics, Lodz, Poland*

23 <sup>l</sup>*Frankfurt Institute for Advanced Studies (FIAS), Frankfurt am Main, Germany*

24 <sup>m</sup>*Department of Physics, University of Bucharest, Bucharest, Romania*

---

## 25 Abstract

The evolution of the muon content of very high energy air showers (EAS) in the atmosphere is investigated with data of the KASCADE-Grande observatory. For this purpose, the muon attenuation length in the atmosphere is obtained to  $\Lambda_\mu = 1256 \pm 85_{-232}^{+229}(\text{syst}) \text{ g/cm}^2$  from the experimental data for shower energies between  $10^{16.3}$  and  $10^{17.0}$  eV. Comparison of this quantity with predictions of the high-energy hadronic interaction models QGSJET-II-02, SIBYLL 2.1, QGSJET-II-04 and EPOS-LHC reveals that the attenuation of the muon content of measured EAS in the atmosphere is lower than predicted. Deviations are, however, less significant with the post-LHC models. The presence of such deviations seems to be related to a difference between the simulated and the measured zenith angle evolutions of the lateral muon density distributions of EAS, which also causes a discrepancy between the measured absorption lengths of the density of shower muons and the predicted ones at large distances from the EAS core. The studied deficiencies show that all four considered hadronic interaction models fail to describe consistently the zenith angle evolution of the muon content of EAS in the aforesaid energy regime.

26 *Keywords:* Cosmic rays, KASCADE-Grande, extensive air showers, muon component,  
27 attenuation length, hadronic interaction models

28 **1. Introduction**

29 Extensive air showers (EAS) are cascades of secondary particles produced by multiple  
30 particle reactions and decays in the atmosphere. These processes are triggered by collisions  
31 of very high energy cosmic rays with the nuclei of the atmosphere. With sophisticated air-  
32 shower detectors, the properties of the EAS are measured with the aim of learning about  
33 the origin and physics of the parent cosmic rays, a task that it is often done by comparing  
34 the EAS data with Monte Carlo simulations. Critical elements of these simulations are the  
35 hadronic interaction models, which rely on physical extrapolations of accelerator measure-  
36 ments taken at lower energies [1]. The distinct phenomenological treatments employed in  
37 the models and the uncertainties of the experimental input data lead to considerable differ-  
38 ences in the predictions of relevant EAS parameters at high energies [1, 2], which introduce  
39 significant model uncertainties when assigning the energy and identifying the nature of the  
40 primary particles from the EAS measurements (see for example [3]). Hence, it is imperative  
41 to check the validity of the hadronic interaction models employed in the study of cosmic  
42 rays.

43 At very high energies and in the kinematical regime relevant for cosmic ray physics, the  
44 performance of hadronic interaction models can be checked by comparing their EAS pre-  
45 dictions with the data of air-shower observatories. Differences between model expectations  
46 and experimental data found in this way can not only serve to constrain the validity of the  
47 models but also to point out some of their deficiencies as a basis for future model improve-  
48 ments. For testing the validity of hadronic interaction models, muons play a particular role.  
49 Muons are created in non-electromagnetic decays of shower hadrons, such as charged pions  
50 and kaons. Once produced, muons decouple immediately from the air shower and travel al-  
51 most in straight lines to the detector with smaller attenuation than that for electromagnetic  
52 and hadronic particles [4]. Studying muons becomes therefore a sensitive and direct way to  
53 probe the hadronic physics [5] and to identify possible deficiencies of hadronic interaction  
54 models [6, 7].

55 In this regard, the present work aims to test the predictions of the high-energy hadronic  
56 interaction models QGSJET-II-02 [8], SIBYLL 2.1 [9], EPOS-LHC[10] and QGSJET-II-04  
57 [11] on the zenith-angle dependence of the muon number in EAS. The study is performed  
58 by measuring the attenuation length of muons in air showers using the constant intensity  
59 cut (CIC) method [12] and by comparing the results with model predictions. The EAS  
60 data were collected with the KASCADE-Grande observatory [13] during the period from  
61 December 2003 to October 2011.

62 The paper is structured as follows: In section 2 a brief description of the experimental  
63 KASCADE-Grande setup and the accuracy of the shower reconstruction at the observatory

---

\*Corresponding author: arteaga@ifm.umich.mx

\*\*Spokesperson KASCADE-Grande: haungs@kit.edu

<sup>1</sup>Now: Head of Division V at KIT - Karlsruher Institut für Technologie, Germany

<sup>2</sup>Now at: Istituto Nazionale di Ricerca Metrologica, INRIM, Torino, Italy

<sup>3</sup>Now at: DLR Oberpfaffenhofen, Germany

<sup>4</sup>Now at: University of Duisburg-Essen, Duisburg, Germany

64 are presented as well as a short description of the selection cuts employed in the study.  
65 Then, in section 3, the characteristics of the Monte Carlo data sets employed for the current  
66 investigation are described and the high-energy hadronic interaction models investigated  
67 in this study are briefly reviewed. The analyses employed to test the hadronic interaction  
68 models are presented in detail in sections 4 and 5. The discussions of the results are reserved  
69 for section 6. Section 7 contains a brief account of the implications of the results for the  
70 features of the hadronic interaction models. In section 8, the conclusions of the present  
71 research are summarized. Finally, the statistical and systematic errors for our results are  
72 listed and discussed in the appendices.

## 73 **2. The KASCADE-Grande observatory**

### 74 *2.1. Experimental set-up*

75 The KASCADE-Grande experiment [13] was an air-shower array devoted to study the  
76 energy spectrum and composition of cosmic rays with energies between  $E = 10^{16}$  and  $10^{18}$  eV,  
77 corresponding to center of mass energies in the range of  $\sqrt{s_{pp}} \approx 4.3$  to 43.3 TeV. The  
78 observatory was installed at the site of the KIT Campus North (49.1° N, 8.4° E, 110 m  
79 a.s.l.), Germany, and consisted of two independent detector subsystems, the Grande and  
80 KASCADE arrays [13]. The former was composed of a  $700 \times 700 \text{ m}^2$  grid of 37 scintillator  
81 stations regularly separated by an average distance of 137 m (see fig. 1) and the latter, by a  
82 smaller and more compact array of 252 shielded and unshielded scintillation detectors spaced  
83 every 13 m over a regular grid of  $200 \times 200 \text{ m}^2$  overall surface. The Grande array provided  
84 ground measurements of the total number of charged particles ( $E > 3 \text{ MeV}$ ),  $N_{ch}$ , at the  
85 EAS front, while the KASCADE array was used to measure the corresponding total number  
86 of muons ( $E_\mu > 230 \text{ MeV}$ ),  $N_\mu$ , among other observables. A more detailed description of  
87 the KASCADE-Grande facility can be found in [13].

### 88 *2.2. EAS reconstruction*

89 Air shower reconstruction in KASCADE-Grande proceeds event-by-event by means of an  
90 iterative algorithm and a careful modeling of the EAS front [13].  $N_{ch}$  is estimated solely from  
91 the Grande data, while  $N_\mu$  is derived from the  $\mu$ -measurements of the KASCADE array. For  
92 the estimation of  $N_{ch}$  a maximum-log-likelihood fit of a modified NKG lateral distribution  
93 function (LDF) [14] is carried out using the densities of charged particles measured by the  
94 Grande array for the event.

95 For the estimation of  $N_\mu$ , in a first step, a calculation of the number of muons detected  
96 in each KASCADE shielded station is performed. This is accomplished by applying a con-  
97 version function (LECF) to the energy deposit recorded in each muon detector, whose main  
98 parameters have a negligible dependence on the shower size and the hadronic interaction  
99 model [13]. In the second and last step, the total number of muons in the EAS is estimated  
100 with the maximum likelihood technique by fitting a Lagutin-Raikin lateral distribution func-  
101 tion with a fixed shape [15] to the data on the number of penetrating particles registered by

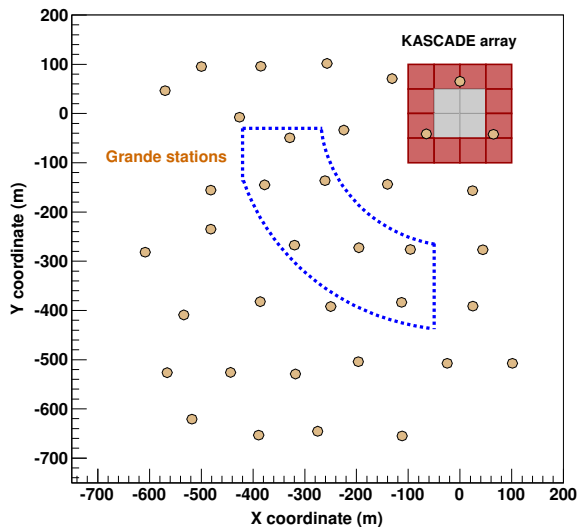


Figure 1: Layout of the KASCADE and the Grande arrays. The circles mark the positions of the 37 Grande detector stations, while the squares indicate the location of the 16 clusters in which were organized the KASCADE detectors. The 12 outer clusters (red squares) of the KASCADE array housed 192 shielded plastic scintillator stations used for measurements of  $N_\mu$ . The dotted contour defines the area selected for the present analysis.

102 the KASCADE detectors:

$$\rho_\mu(r) = N_\mu \cdot \frac{0.28}{r_0^2} \left(\frac{r}{r_0}\right)^{p_1} \left(1 + \frac{r}{r_0}\right)^{p_2} \left(1 + \left(\frac{r}{10 \cdot r_0}\right)^2\right)^{p_3} \quad (1)$$

103 with  $r$  the radial distance from the EAS core measured at the shower plane. The parameters  
 104 of the above equation are  $p_1 = -0.69$ ,  $p_2 = -2.39$ ,  $p_3 = -1.0$  and  $r_0 = 320$  m [13]. They were  
 105 obtained calibrating the function with the results of CORSIKA/QGSJET-01 simulations,  
 106 in particular, by averaging the fits to simulated protons and iron nuclei with energies of  
 107  $10^{16}$  and  $10^{17}$  eV. Fixing the shape of the muon lateral distribution obeys to the limited  
 108 statistics available from the muon detectors. If relaxing this constraint on the LDF shape,  
 109 the fit becomes unstable.

110 The resolution achieved by the whole fitting procedure is  $\lesssim 15$  % for  $N_{ch}$  and  $\lesssim 25$  % for  
 111  $N_\mu$ . The first value was estimated in a model independent way [13] and the second one, from  
 112 MC simulations using the models under study (see Appendix A). For the upcoming analysis,  
 113 in order to improve the accuracy of the muon number and consequently on the determination  
 114 of the muon attenuation length,  $N_\mu$  was corrected for experimental and reconstruction effects  
 115 using a correction function (c.f. Appendix A). The latter was built from MC simulations  
 116 based on the QGSJET-II-02 model. The choice of the MC model is not relevant for this  
 117 task, because the correction is almost independent of the high-energy hadronic interaction  
 118 model. After corrections, the mean  $N_\mu$  systematic errors are reduced to  $\lesssim 10$  % with a weak  
 119 dependence on the core position, the shower size, the muon size and the shower zenith angle

120 in the full efficiency regime and, in particular, on the selected data sample.

### 121 *2.3. Selection cuts and description of the data*

122 Several selection cuts were developed in order to reduce the effect of systematic uncer-  
123 tainties on the reconstructed shower observables, mainly on  $N_\mu$ . These selection criteria  
124 were applied indistinctly to experimental data and simulated events.

125 First, selected events had to satisfy a 7/7 Grande hardware trigger (six of a hexagonal  
126 shape and the central one) and activate more than 11 Grande stations from a minimum num-  
127 ber of 36 working Grande stations. Besides, all KASCADE detector clusters were required  
128 to be in operation during the data acquisition of the events. The quality of the reconstruc-  
129 tion of the selected sample was assured by considering only events that passed successfully  
130 the standard reconstruction procedure of KASCADE-Grande. In addition, the selection for  
131 the present analysis included only events with their cores located at a distance between 270  
132 and 440 m from the KASCADE center and within a central area of  $8 \times 10^4 \text{ m}^2$  inside the  
133 Grande array (c.f. fig. 1). With this cut not only edge effects were avoided but also a  
134 significant reduction of the  $N_\mu$  systematic uncertainties was achieved. In particular, events  
135 with a large contribution from the electromagnetic punch-through effect were eliminated.  
136 Showers with zenith angles greater than  $40^\circ$  were also removed as they have a large pointing  
137 error. A further constraint on the data was set by introducing the limit  $\log_{10} N_\mu > 4.6$  on  
138 the reconstructed (not corrected yet) muon number for EAS. This cut helped to discard a  
139 number of events below the efficiency threshold irrelevant for the present analysis.

140 After these selection cuts, the full trigger and reconstruction efficiency of the KASCADE-  
141 Grande experiment is achieved at threshold energies around  $\log_{10}(E/\text{GeV}) = 7.00 \pm 0.20$   
142 and corrected muon numbers  $\log_{10} N_\mu = 5.00 \pm 0.20$ , according to MC simulations. The  
143 small uncertainties originate from the unknown primary composition, the arrival direction  
144 and the hadronic interaction model involved. For the selected events, the mean core and  
145 pointing resolutions of KASCADE-Grande are better than 8 m and  $0.4^\circ$ , respectively, and  
146 are almost independent of the radial distance to the KASCADE array. The application  
147 of the selection criteria to the KASCADE-Grande data yielded a data set with 2,744,950  
148 shower events corresponding to a total exposure of  $2.6 \times 10^{12} \text{ m}^2 \cdot \text{s} \cdot \text{sr}$ .

## 149 **3. Monte Carlo simulations**

150 MC data were generated using simulations of the EAS development and of the response of  
151 the detectors of the KASCADE-Grande array. In order to simulate the EAS evolution in the  
152 atmosphere, the CORSIKA code [16] was used without employing the thinning algorithm.  
153 The U.S. standard atmosphere model as parameterized by J. Linsley (c.f. [16] and references  
154 therein) was employed, as the mean of the local RMS air pressure values at the site of the  
155 KASCADE-Grande observatory is close to the magnitude predicted by the abovementioned  
156 model [17].

157 The physics of the hadronic interactions was simulated using Fluka [18] at low energies  
158 ( $E_h < 200 \text{ GeV}$ ) combined with QGSJET-II-02, SIBYLL 2.1, QGSJET-II-04 and EPOS-  
159 LHC as different alternatives to model the high energy regime. MC showers were generated

160 for the KASCADE-Grande location and followed until they reach the detector level. The  
 161 CORSIKA output was injected in a GEANT 3.21 [19] based code, where the response of the  
 162 KASCADE-Grande components were simulated in full detail and stored in data files, which  
 163 have the same format as the experimental data. The MC files were then processed with the  
 164 same KASCADE-Grande reconstruction program that was applied to the measured data.  
 165 This way, systematic uncertainties owing to the use of different reconstruction algorithms  
 166 were avoided.

167 The energy spectrum of the events in the MC data sets ranges from  $10^{16}$  until  $10^{18}$  eV  
 168 and follows an  $E^{-2}$  law. However, weights had to be introduced and applied to the MC  
 169 data to simulate more realistic spectra (see, for example, [20, 21]) with  $\gamma = -2.8, -3, -3.2$ .  
 170 Regarding the spatial distribution of the MC events, they are isotropically distributed and  
 171 their cores at ground are homogeneously scattered over the full array. Shower simulations  
 172 are done up to zenith angles of  $42^\circ$  with no restriction for the azimuthal angle. Concerning  
 173 composition, MC data contain individual sets for different representative primaries: hydro-  
 174 gen (H), helium (He), carbon (C), silicon (Si) and iron (Fe) nuclei, with roughly the same  
 175 statistics. An additional data set for each interaction model was also included simulating  
 176 a mixed composition scenario, where the above elements are present in equal abundances.  
 177 The final QGSJET-II-02 data set with the five primaries contains 1.9 million events, while  
 178 the corresponding data files for the other models comprise roughly 1.2 million events for  
 179 SIBYLL 2.1, 1.3 million events for QGSJET-II-04 and 2.2 million events for EPOS-LHC.

180 Several differences are expected among the predictions of the various hadronic interac-  
 181 tions models for the KASCADE-Grande energy range at the altitude of the observatory.  
 182 Comparative studies performed for KASCADE-Grande showed that QGSJET-II-02 pro-  
 183 duces a lower muon content in vertical EAS than the most recent models QGSJET-II-04  
 184 and EPOS-LHC, but more muons than SIBYLL 2.1 (e.g., at  $E \sim 10^{17}$  eV, they amount  
 185 to  $\approx 13\%$  and  $21\%$  for the first two cases, respectively, and to  $7\%$  for the last one). On  
 186 the other hand, it was found that QGSJET-II-02 predictions for the  $N_\mu/N_{ch}$  ratio in verti-  
 187 cal showers are smaller than the corresponding QGSJET-II-04 and EPOS-LHC estimations  
 188 ( $18\%$  and  $19\%$ , respectively, at  $E \sim 10^{17}$  eV). However, the QGSJET-II-02 ratios turned  
 189 out to be almost equal to the SIBYLL 2.1 derived ones. The main reasons behind the  
 190 muon enhancement in the current version of QGSJET-II-04 are the larger  $\pi^\pm$  production  
 191 in pion-air interactions and the harder pion spectra [22]. The latter is due to an increased  
 192 forward  $\rho^0$  production in pion-nucleus collisions, compared to  $\pi^0$  generation, which enhances  
 193 via the decay mode  $\rho^0 \rightarrow \pi^+\pi^-$  the relative proportion of charged pions in EAS and leads  
 194 to an increase of the shower muon content [22]. In EPOS-LHC, an additional increase of  
 195 the muon production originates from an enhanced production of baryon-antibaryon pairs in  
 196 pion-nucleus collisions, which effectively increases the number of hadron generations in the  
 197 atmospheric nuclear cascades [23]. For more details concerning the models, predictions for  
 198 other EAS observables, and theoretical approaches see references [22, 23].

199 **4. The muon attenuation length**

200 We focus the present analysis to the calculation of the attenuation length of the number  
 201 of shower muons in the atmosphere,  $\Lambda_\mu$ , as an appropriate physical quantity to study the  
 202 evolution of the muon content of EAS in the atmosphere. This is an easy and direct way  
 203 to compare the  $N_\mu$  evolution observed in EAS with the predictions from MC simulations.  
 204 In general, the EAS attenuation length is a quantity that measures the degree of effective  
 205 attenuation that a given air-shower component or observable undergoes in the atmosphere.  
 206 In particular, it is sensitive to the longitudinal development of the EAS [24] and it is a-  
 207 fected by the inelastic hadronic cross section of the primary particle [25] and the underlying  
 208 mechanisms of particle production in the shower [23]. The EAS attenuation length is, in  
 209 consequence, a physical quantity that encloses a large amount of information about the  
 210 generation and development of the air shower.

211 Alternative definitions exist for the EAS attenuation length depending of the shower  
 212 component and the applied experimental technique (see for example [24, 25] and references  
 213 therein). Here, we will use the approach based on the Constant Intensity Cut (CIC) method  
 214 [12], as it is well-established and independent of the hadronic interaction model. Pioneering  
 215 work using the CIC method along with the  $N_\mu$  data can be found for example in [26] and  
 216 [27] (see also [24] and references therein). The approach has been exploited for a number  
 217 of reasons at some EAS observatories, e.g. for the reconstruction of the energy spectrum  
 218 of cosmic rays [27], the calculation of the  $p$ -Air cross section [26], the test of hadronic  
 219 interaction models [27] and the extraction of  $\Lambda_\mu$  [24, 26, 27]. However, in the latter case, the  
 220 different experimental conditions, muon energy thresholds and EAS reconstruction methods  
 221 of the observatories as well as the distinct column depths of the sites prevent us to compare  
 222 those early measurements of  $\Lambda_\mu$  with that from the present paper.

223 The aim of the CIC method is to provide a way to relate data from different zenith angles  
 224 at roughly the same primary energies, without any reference to MC simulations. This is  
 225 achieved through the calculation of attenuation curves at fixed shower rates. The CIC  
 226 method is based on the assumption that the arrival distribution of cosmic rays is isotropic  
 227 so that the observed intensity of primary particles with the same energy is independent of  
 228 the zenith angle or the slant depth.

229 In order to apply the CIC method, in the first instance, data were grouped into five  
 230 zenith-angle intervals with roughly the same aperture (see fig. 2, left). Then, for each  
 231 angular bin the corresponding integral muon intensity<sup>5</sup>  $J(> N_\mu, \theta)$  is estimated according  
 232 to the following formula:

$$J(> N_\mu, \theta) = \int_{N_\mu} \Phi(N_\mu, \theta) dN_\mu, \quad (2)$$

233 where  $\Phi(N_\mu, \theta)$  represents the differential muon shower size spectrum.

234 Five cuts are applied on  $J(> N_\mu, \theta)$  at different constant integral intensities in order to  
 235 select showers with the same frequency rate at distinct zenith angles. This procedure is

---

<sup>5</sup>Defined as the number of showers detected above  $N_\mu$  per unit solid angle, unit area and unit of time.

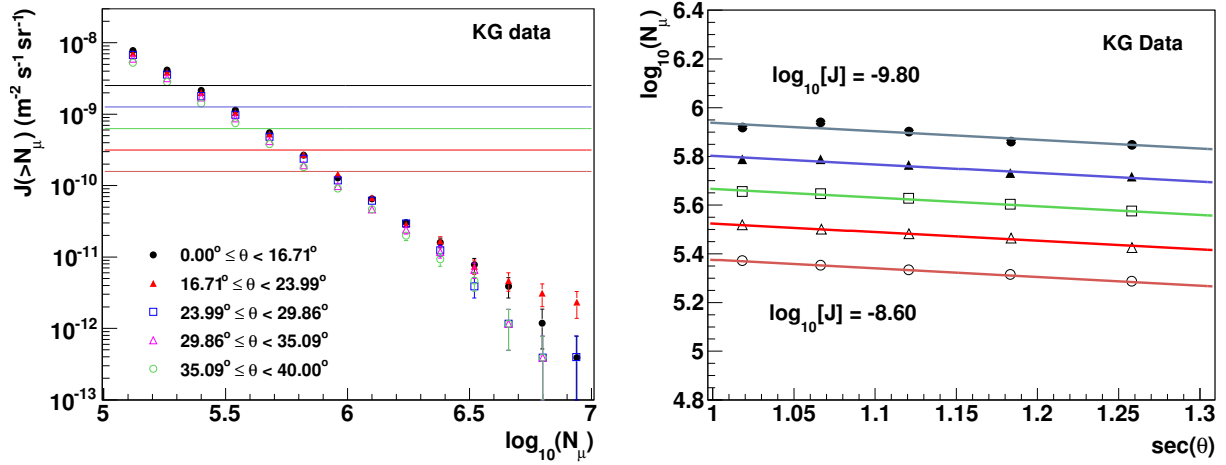


Figure 2: Left: Muon integral intensities for five zenith-angle intervals derived from the measurements with KASCADE-Grande, where the muon correction function is already applied. Error bars represent statistical uncertainties. The CIC employed are shown as horizontal lines. Right: Muon attenuation curves obtained by applying the CIC to the KASCADE-Grande integral spectra,  $J_\mu$ . The cuts decrease from the bottom to the top in units of  $\Delta \log_{10}[J/(\text{m}^{-2} \cdot \text{s}^{-1} \cdot \text{sr}^{-1})] = -0.30$ . Errors are smaller than the size of the symbols. They take into account statistical uncertainties, errors from interpolation as well as the correlation between adjacent points when interpolation was applied.

236 performed within the interval  $\log_{10} N_\mu \approx [5.2, 6.0]$  of full efficiency and maximum statistics  
 237 as shown in fig. 2 (left).

238 After that, the intersections of each cut with the integral spectra for the different angular  
 239 bins are found<sup>6</sup>. Then for each constant intensity cut, a muon attenuation curve  $\log_{10} N_\mu(\theta)$   
 240 is build using the corresponding set of intersection points. The results are displayed on the  
 241 right plot of fig. 2 for all CIC cuts employed in the study. These attenuation curves describe  
 242 roughly the way in which the muon content of an average EAS evolves in the atmosphere  
 243 for different primary energies. Finally, in order to extract the value of the muon attenuation  
 244 length ( $\Lambda_\mu$ ) that best describes our data, a global fit via a  $\chi^2$ -minimization is applied to the  
 245 set of attenuation curves using

$$N_\mu(\theta) = N_\mu^\circ e^{-X_0 \sec \theta / \Lambda_\mu}, \quad (3)$$

246 with a common  $\Lambda_\mu$ , where  $X_0 = 1022 \text{ g/cm}^2$  is the average atmospheric depth for verti-  
 247 cal showers at the location of the experiment and  $N_\mu^\circ$  is a normalization parameter to be  
 248 determined for each attenuation curve. The analysis of both the MC and measured data  
 249 have shown that it is possible to use a single  $\Lambda_\mu$  for the entire  $N_\mu$  range, as the standard  
 250 deviation of the results obtained when fitting individually the attenuation curves are smaller  
 251 than  $\sim 3\%$  in each case.

<sup>6</sup>When necessary, interpolation between two adjacent points along the same intensity was applied by means of a simple power-law expression.

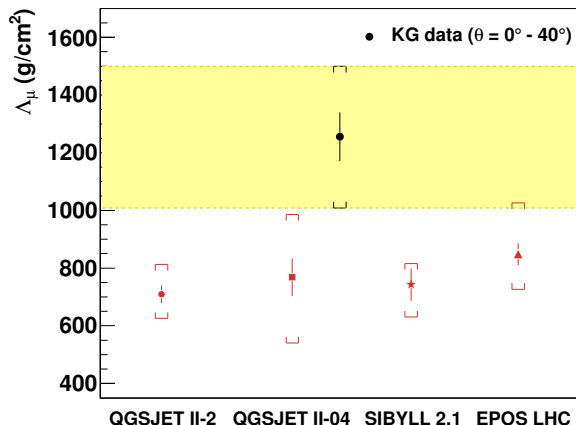


Figure 3: Muon attenuation lengths extracted from Monte Carlo (points below shadowed area) and experimental data (upper black circle). Error bars indicate statistical uncertainties, while the brackets represent the total errors (systematic plus statistical errors added in quadrature). The shadowed band covers the total uncertainty estimated for the experimental result.

252 The value of the muon attenuation length of EAS measured with the KASCADE-Grande  
 253 array is presented in table 1 and fig. 3 together with the values extracted from MC data  
 254 by applying the same analysis. The quoted values for  $\Lambda_\mu$  in case of MC data correspond  
 255 to the predictions of different hadronic interaction models tested under the assumption of  
 256 a mixed composition scenario with  $\gamma = -3$ . It must be mentioned that simulated data has  
 257 been normalized in such a way that MC muon size spectra for vertical showers are equal  
 258 to the measured one around  $\log_{10}(N_\mu) = 5.5$ . We should also add that the mean primary  
 259 energies of the shower events lying along the attenuation curves shown in fig. 3 cover the  
 260 energy intervals  $\log_{10}(E/\text{GeV}) = [7.4, 8.0]$ ,  $[7.3, 7.9]$ ,  $[7.4, 8.0]$  and  $[7.3, 7.9]$  according to the  
 261 QGSJET-II-02, QGSJET-II-04, SIBYLL 2.1 and EPOS-LHC models, respectively. These  
 262 energy assignments were estimated from  $N_\mu$  using power-law formulas calibrated with MC  
 263 data for each zenith-angle interval. A primary cosmic ray spectrum characterized by a mixed  
 264 composition and a spectral index  $\gamma = -3$  was used for the energy calibration. Returning  
 265 to table 1, results are accompanied by their statistical and systematic uncertainties. The  
 266 experimental systematic error includes (a detailed discussion can be found in Appendix B):

- 267 • uncertainty resulting from the CIC method;
- 268 • uncertainty owing to the size of the zenith-angle intervals;
- 269 • uncertainty in the parameters of the muon correction function;
- 270 • systematic bias of the corrected muon number and its model and composition dependence;
- 271
- 272 • and uncertainties associated with the EAS core position relative to the center of the
- 273 KASCADE muon array.

274 In addition, the MC systematic error includes uncertainties associated with the spectral  
 275 index and primary composition.

Table 1: Muon attenuation lengths extracted from Monte Carlo and experimental data.  $\Lambda_\mu$  is presented along with their statistical and systematic errors (in order of appearance). Also given are deviations (in units of  $\sigma$ ) of the measured  $\Lambda_\mu$  from the predictions of different hadronic interaction models. The one-tailed confidence levels (CL) that the measured value is in agreement with the MC predictions are also presented.

	QGSJET-II-02	QGSJET-II-04	SIBYLL 2.1	EPOS-LHC	KG data
$\Lambda_\mu$ (g/cm <sup>2</sup> )	$709 \pm 30^{+99}_{-78}$	$768 \pm 65^{+208}_{-219}$	$743 \pm 56^{+47}_{-98}$	$848 \pm 38^{+174}_{-115}$	$1256 \pm 85^{+229}_{-232}$
Deviation ( $\sigma$ )	+2.04	+1.48	+1.99	+1.34	
CL (%)	2.08	6.96	2.34	9.07	

276 From fig. 3, it is observed that the measured  $\Lambda_\mu$  lies above the MC predictions. The  
277 deviations of the experimental value from the MC expectations are shown in table 1 along  
278 with the confidence levels (CL) for agreement with the model estimations. From both table 1  
279 and fig. 3, it can be seen that the pre-LHC models QGSJET-II-02 and SIBYLL 2.1 show the  
280 largest discrepancies with deviations at the level of  $+2.04\sigma$  and  $+1.99\sigma$ , respectively. The  
281 corresponding CL's are 2.08 % and 2.34 % and indicate that the probability of agreement  
282 between experiment and the expectations is low for these cases. On the other hand, just  
283 slight discrepancies are found for the post-LHC models QGSJET-II-04 and EPOS-LHC, with  
284  $+1.48\sigma$  and  $+1.34\sigma$ , respectively, which imply that both predictions are each in reasonably  
285 agreement with the measured value with CL's of 7 % and 9 % , respectively. In spite of this,  
286 however, the fact that central values of the QGSJET-II-04 and EPOS-LHC predictions are  
287 still below the experimental data could mean that more work is still needed within these  
288 post-LHC models to give also a precise description of the KASCADE-Grande air-shower  
289 results (this seems to be the case as revealed by the complementary study performed in  
290 section 5).

291 Potential sources of systematic errors which could explain the observed deviation between  
292 the expectations and the measurement were studied and are presented in Appendix C.  
293 Special attention was given to systematic shifts of  $\Lambda_\mu$  produced by instrumental effects,  
294 reconstruction procedures, EAS fluctuations and environmental effects, e.g., the aging of the  
295 muon detectors, the core position and arrival angle resolutions of the apparatus, errors in the  
296 reconstructed number of muons from uncertainties in the deposited energy per KASCADE  
297 shielded detector, the uncertainty in the  $N_\mu$  correction function, fluctuations on the number  
298 of registered particles per muon station, the evolution of the chemical composition of cosmic  
299 rays in the energy range considered and the influence of local variations of the atmospheric  
300 temperature and pressure. However, the analyses have shown that the disagreement on  $\Lambda_\mu$   
301 between MC predictions and the experimental measurement can not be ascribed to any of the  
302 above sources. We also investigated the uncertainty in the shape of the muon LDF employed  
303 with the EAS data. Here we show that it contributes to the discrepancy, but it is not the  
304 leading effect. Therefore, the observed difference very likely originates from deficiencies of  
305 the muon predictions of the high-energy hadronic interaction models underlying our studies.

306 The fact that the experimental value of  $\Lambda_\mu$  is greater than the expected values from MC

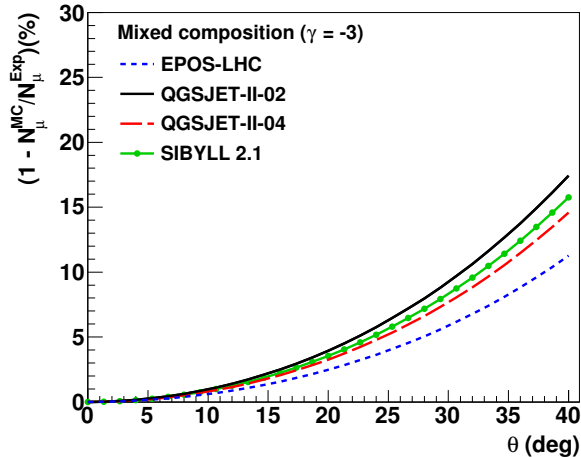


Figure 4: Relative differences in percentage between the measured muon content of EAS and the corresponding predictions of MC models under the assumption that the actual  $N_\mu$  in vertical showers is well described by the models. Differences are presented as a function of the zenith angle according to equation (4).

307 simulations implies that the observed air showers attenuate more slowly in the atmosphere  
 308 than the simulated ones. It is difficult at this point to quantify the influence of such an  
 309 effect on the differences between the predicted and measured muon content of air showers at  
 310 large zenith angles. However, a naive estimation can be done by assuming that for vertical  
 311 showers the MC predictions for the muon number agree with the measured values at the  
 312 same energy. Using equation (3), it is found that the  $N_\mu$  differences,  $\Delta_\mu$ , expected between  
 313 measurements and MC predictions at different zenith angles, are given by

$$\Delta_\mu = 1 - N_\mu^{MC}(\theta)/N_\mu^{Exp}(\theta) = 1 - e^{-X_0 \cdot (\sec \theta - 1) \cdot (1/\Lambda_\mu^{MC} - 1/\Lambda_\mu^{Exp})}, \quad (4)$$

314 where the simulated attenuation curves have been normalized at  $\theta = 0^\circ$  in such a way that  
 315  $N_\mu^{MC}(0^\circ) = N_\mu^{Exp}(0^\circ)$ . Predictions do not take into account systematic uncertainties from  
 316 the reconstruction method, experimental errors or the analysis technique. From fig. 4 it is  
 317 observed that the  $\Delta_\mu$  differences increase exponentially for inclined showers becoming as  
 318 high as 18% at  $\theta = 40^\circ$ . Note that QGSJET-II-02 gives the highest differences due to its  
 319 lower muon attenuation length (c.f. table 1). On the contrary, the smallest differences are  
 320 found in case of EPOS-LHC. In general, the results shown in fig. 4 imply that a higher  
 321  $N_\mu$  should be expected in data than in MC events for air showers arriving at high zenith  
 322 angles. Of course, it could also happen that both measurements and predictions are in  
 323 better agreement at high zenith angles, which would suggest a smaller muon content for the  
 324 actual vertical EAS in comparison with simulations. To settle down the question a direct  
 325 measurement of the shower energy, independent of MC calibrations as much as possible,  
 326 would be necessary. Unfortunately this is not the case for KASCADE-Grande, where the  
 327 energy is estimated in a model dependent way from the measured EAS observables and has  
 328 an uncertainty associated with the primary composition [21].

## 329 5. The muon absorption length

330 To have a better understanding of the observed deviations and to avoid some of the  
 331 sources of systematic uncertainties discussed above, we study now the zenith-angle evolution  
 332 of the muon component of EAS using the mean local density of muons instead of the  $N_\mu$   
 333 observable for showers with about the same primary energy. The quantity reflecting this  
 334 evolution is the muon absorption length,  $\alpha_\mu$ , also called the attenuation length of  $\rho_\mu(r)$  [28].  
 335 To proceed in a model independent way, the CIC method is applied again, however, on  $N_{ch}$   
 336 in place of the muon number, since the former has a lower systematic uncertainty and its  
 337 observed zenith-angle evolution is in better agreement with the MC calculations. Besides,  
 338 because using  $N_{ch}$  as an energy estimator provides a way to avoid possible systematic errors  
 339 associated with  $N_\mu$  that might contribute to the discrepancy observed on the muon content  
 340 of EAS. The only drawback is that  $N_{ch}$  is subject to bigger shower fluctuations than  $N_\mu$  at  
 341 the same energy, which causes a reduction of the measured  $\alpha_\mu$  for decreasing values of the  
 342 shower size. This effect is the result of a bias driven mainly by the influence of shower-to-  
 343 shower fluctuations of  $N_{ch}$  on the EAS selection. In order to reduce it, only data with large  
 344  $N_{ch}$  were selected for the present study, in particular, with  $E \approx 10^{17}$  eV.

345 Using the CIC method,  $\Lambda_{ch}$  was estimated (see Appendix D) and afterwards employed  
 346 to calculate the equivalent charged number of particles,  $N_{ch}^{CIC}$ , at a zenith angle of reference,  
 347  $\theta_{ref} = 22^\circ$  (the mean of the zenith-angle distribution of experimental data). This shower size  
 348 observable was then used to select events in the interval  $\log_{10} N_{ch}^{CIC} = [7.04, 7.28]$ , roughly  
 349 corresponding to the energy region<sup>7</sup> from  $\approx 10^{16.9}$  to  $\approx 10^{17.2}$  eV. Events were further  
 350 classified into five zenith angle intervals (with the same ranges used in the analysis of  $\Lambda_\mu$ )  
 351 and within each of these bins, the mean muon densities at the shower plane,  $\bar{\rho}_\mu(r)$ , were  
 352 obtained. The procedure consists of dividing the shower plane in concentric rings (40 m width  
 353 each) and then, for each  $\theta$  interval and radial bin, in dividing the total number of detected  
 354 muons by the corresponding sum of projected effective areas of the muon detectors registered  
 355 as active during the data taking of each selected event. No corrections for atmospheric  
 356 attenuation effects were included when passing the muon data from the coordinate system  
 357 of the detector to that of the shower plane. The experimental results for the mean LDF of  
 358 muons within the above ranges are presented in fig. 5.

359 To quantify  $\alpha_\mu(r)$ , absorption curves  $\log_{10} \bar{\rho}_\mu(r)$  vs  $\sec(\theta)$  were further calculated. The  
 360 curves were obtained from the  $\bar{\rho}_\mu(r)$  distributions by applying several cuts at fixed distances  
 361  $r$  from the EAS core at the shower plane (see fig. 5, for example). Cuts were applied in  
 362 the interval  $r = [180 \text{ m}, 380 \text{ m}]$ , where statistical fluctuations are low. For each absorption  
 363 curve, the muon absorption length,  $\alpha_\mu(r)$ , was then estimated by fitting the data with the  
 364 following relation:

$$\bar{\rho}_\mu(r, \theta) = \bar{\rho}_\mu^\circ(r) e^{-X_0 \sec \theta / \alpha_\mu(r)}, \quad (5)$$

---

<sup>7</sup>In particular, for a mixed composition assumption and a power-law energy spectrum  $\propto E^{-3}$ , the  $N_{ch}^{CIC}$  intervals include data with mean energy in the ranges of  $\log_{10}(E/\text{GeV}) = [7.91, 8.14]$ ,  $[7.97, 8.20]$ ,  $[7.95, 8.16]$  and  $[7.89, 8.10]$  for QGSJET-II-02, QGSJET-II-04, SIBYLL 2.1 and EPOS-LHC, respectively. Energy estimations were based in MC calibrated relations between the primary energy and the shower size for  $\theta = [21^\circ, 23^\circ]$ .

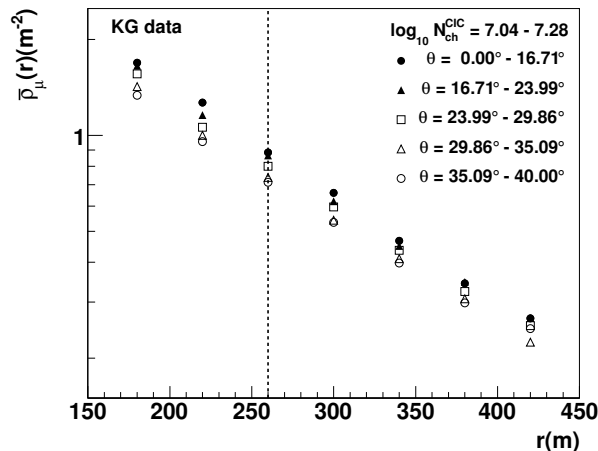


Figure 5: Mean lateral distributions of measured local muon densities for several zenith-angle intervals and the shower size range  $\log_{10} N_{ch}^{CIC} = [7.04, 7.28]$ . The vertical line is an example of the cuts applied at a fixed radius to extract the corresponding muon absorption lengths. Statistical error bars of the data points are smaller than the size of the markers.

365 where  $\bar{\rho}_\mu^o(r)$  is a normalization parameter.

366 Fig. 6 shows the values of  $\alpha_\mu$  extracted from the KASCADE-Grande data for the chosen  
 367  $N_{ch}^{CIC}$  interval together with the predictions of MC simulations for different hadronic inter-  
 368 action models. The MC values were calculated for a mixed composition assumption and a  
 369 primary spectral index of  $\gamma = -3$ . The predicted  $\alpha_\mu$  curves are accompanied by shadowed  
 370 error bands that take into account the systematic errors due to both, composition and spec-  
 371 tral index uncertainties in the primary spectrum. The errors associated with the spectral  
 372 index were obtained by repeating the calculations with  $\gamma = -2.8$  and  $-3.2$ , while the errors  
 373 due to composition were estimated by considering the distinct primary nuclei simulated in  
 374 our MC data samples.

375 It is evident from fig. 6 that the evolution of the measured  $\bar{\rho}_\mu(r)$  distributions in the  
 376 atmosphere is not in agreement with the expectations of the hadronic interaction models  
 377 studied in this work. We found that the measured  $\alpha_\mu$  tends to stay above the MC predictions  
 378 and that there is only a marginal agreement between the models and the experimental data  
 379 for radial distances closer to the shower core. Fig. 6 shows that the differences between the  
 380 measurements and the model calculations rise with the lateral distance to the core of the  
 381 EAS. Strikingly, the  $\Lambda_\mu$  parameter exhibits a similar radial behavior as it was verified during  
 382 the study of systematic errors (see Appendix B) and in further analyses based on muon data  
 383 around the EAS core<sup>8</sup>. In consequence, we can conclude that the inconsistencies observed  
 384 in the study of  $\Lambda_\mu$  are still present in the data for the local muon densities. Therefore, the

<sup>8</sup>We selected events with EAS cores within 58 – 250 m from the center of the KASCADE array and applied the whole analysis described in this paper to extract  $\Lambda_\mu$  from the MC and the experimental data. For QGSJET-II-02, we found a negligible variation of  $\Lambda_\mu$  with respect to the corresponding value of table 1, but for the measured data a reduction of almost  $\approx 400 \text{ g/cm}^2$  was obtained, increasing the agreement with model predictions.

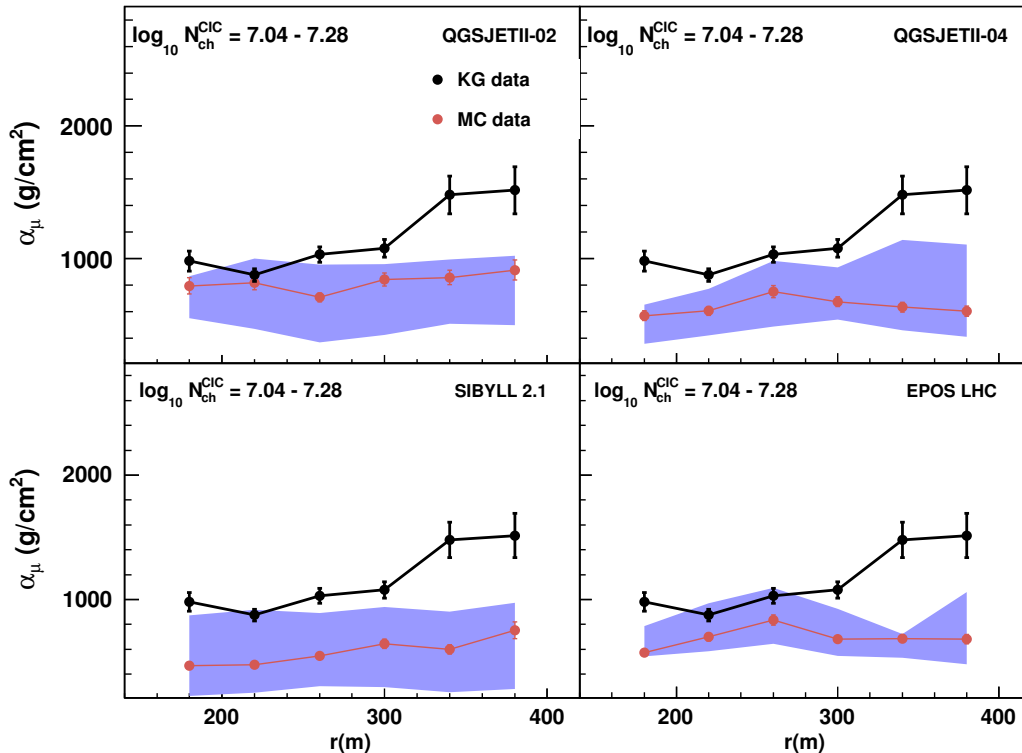


Figure 6: Muon absorption lengths for measured (black) and simulated EAS data (red) plotted against the radial distance at the shower disk plane for the given  $\log_{10} N_{ch}^{CIC} = 7.04 - 7.28$  interval. The blue bands represent the systematic uncertainties due to composition and the spectral index of the primary cosmic ray flux (see text). The error bars represent the uncertainties from the fits. Note that, in some cases, for MC data points the error bars are smaller than the size of the markers.

385 referred disagreements are not an artefact of the treatment of the  $N_{\mu}$  data or the way in  
 386 which this parameter is estimated from the particle densities at the muon detectors.

387 Thus, in view of the above results, it seems entirely justifiable to say that the discrep-  
 388 ancies observed in the analysis of the local  $\bar{\rho}_{\mu}(r)$  distributions are the main responsible for  
 389 the disagreement discovered in the analysis of  $\Lambda_{\mu}$ . This asseveration was further supported  
 390 by additional tests carried out with Monte Carlo data (c.f. Appendix C), in which we ob-  
 391 served that after increasing  $\alpha_{\mu}$  in MC simulations to reproduce the measured value, the  
 392 experimental result of  $\Lambda_{\mu}$  can be recovered from the MC events.

393 Here, it is important to add that despite the above deviations, the measured muon  
 394 densities for  $\theta < 40^{\circ}$  along the corresponding CIC curve are still bracketed by the estimations  
 395 from the QGSJET-II-02, QGSJET-II-4 and EPOS-LHC models for proton and iron nuclei,  
 396 at least for the interval  $r = [180 \text{ m}, 440 \text{ m}]$ . This is demonstrated in fig. 7. In contrast, for  
 397 SIBYLL 2.1, the situation is different, model predictions for proton and iron primaries do  
 398 not contain the measured data for inclined showers ( $35.1^{\circ} \leq \theta \leq 40^{\circ}$ ) within the shower size  
 399 range  $\log_{10} N_{ch}^{CIC} = 7.04 - 7.28$ . This result reveals an additional deficiency of the SIBYLL  
 400 2.1 model. However, it does not allow us to determine whether the model underestimates

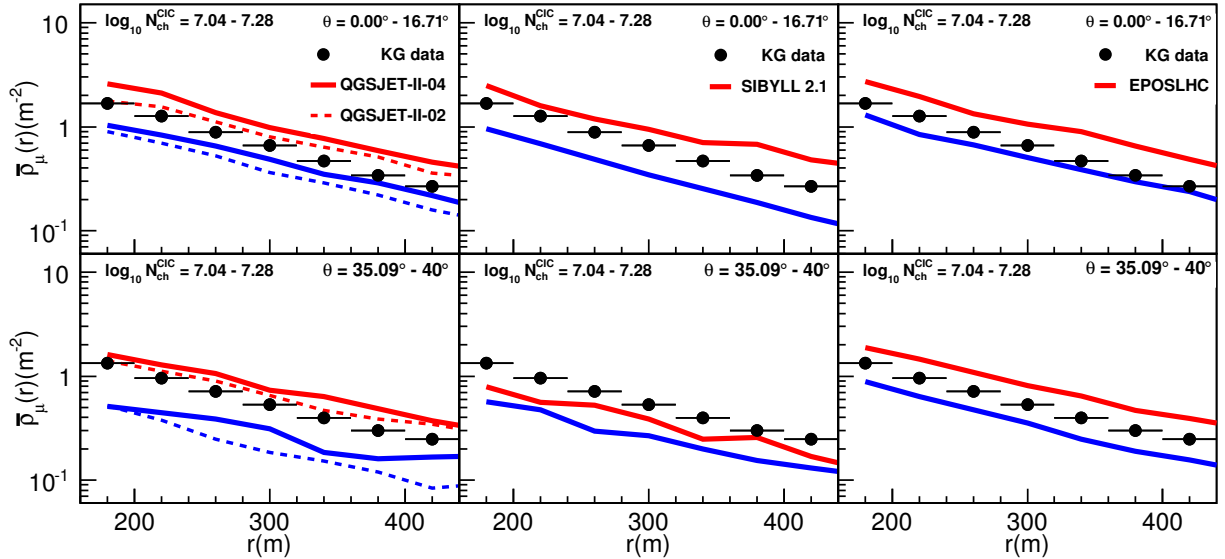


Figure 7: Mean muon lateral distributions of EAS for the bin  $\log_{10} N_{ch}^{CIC} = [7.04, 7.28]$  and two different zenith-angle intervals. The solid points represent the experimental data and the lines the predictions from the models. Left column: QGSJET-II models; middle: SIBYLL 2.1; right: EPOS-LHC. For each model, results are shown for protons and iron nuclei (lower and upper lines, respectively). Statistical error bars of the data points are smaller than the size of the markers.

401 or overestimates the muon content of EAS. The reasons are that, first, the result depends  
 402 on the reference angle that is used to find  $N_{ch}^{CIC}$  and, second, the energy calibration in  
 403 KASCADE-Grande is model and composition dependent.

## 404 6. Discussion of the measurements

405 The attenuation length of  $N_{\mu}$  was measured at KASCADE-Grande for energies between  
 406  $10^{16.3}$  and  $10^{17.0}$  eV. The measured value is higher than the predictions of QGSJET-II-  
 407 02 and SIBYLL 2.1 but just exceeds slightly the model calculations for EPOS-LHC and  
 408 QGSJET-II-04 (see table 1). The presence of such deviations was confirmed by the study of  
 409 the  $\alpha_{\mu}(r)$  coefficients of the  $\bar{\rho}_{\mu}$  distributions measured locally at KASCADE-Grande around  
 410  $E = 10^{17}$  eV. This analysis showed that the actual  $\alpha_{\mu}(r)$  parameters become increasingly  
 411 bigger than the predicted MC values at large distances from the EAS core (c.f. fig. 6). The  
 412 anomaly seems to be mainly associated to a bad description of the  $\theta$  dependence of the muon  
 413 LDF's by the MC simulations (see Appendix C.4 and Appendix C.5). On the grounds of  
 414 the above results, a general conclusion is derived that the high-energy hadronic interaction  
 415 models here analyzed can not describe consistently all the muon data of EAS measured with  
 416 the KASCADE-Grande array at different zenith angles<sup>9</sup>.

<sup>9</sup>Recently the post-LHC version of the SIBYLL model was released [29]. The performance of this model at KASCADE-Grande is still under investigation. Results will be presented elsewhere.

417 When extracting  $\Lambda_\mu$  from the experimental data some input from the MC models was  
 418 unavoidable. First, through the lateral energy conversion function (LECF) to estimate the  
 419 number of muons detected per muon station, then through the muon LDF employed to  
 420 estimate  $N_\mu$  and finally, through the muon correction function introduced to correct  $N_\mu$  for  
 421 systematic biases. One may suppose that the inclusion of such functions could invalidate  
 422 the comparison between data and MC predictions. Nevertheless, the model-experiment  
 423 comparison of the EAS data is completely justified, as we have processed and analysed both  
 424 the experimental and simulated events in identical ways using the same MC functions. Under  
 425 the foregoing procedure, however, it may become unclear whether the observed discrepancies  
 426 are due to the studied phenomenon or to a misleading description of the aforesaid functions  
 427 by the hadronic interaction models.

428 The possibility that the MC based functions introduce the observed deviations in the  $\Lambda_\mu$   
 429 results seems to be weakened in view of the small model dependence that these functions  
 430 show (c.f. [13] and Appendix A) and due to the small variations that the relative systematic  
 431 errors of  $N_\mu$  exhibit with the model (see fig. A1, left). These kind of arguments are often  
 432 invoked to validate some present studies (see, e.g. [7]). However, one can argue that they  
 433 do not constitute a solid proof against the possibility being discussed. In this regard, it is  
 434 desirable to rely on additional analyses. For this reason, we have run the complementary  
 435 tests performed in section 5 and Appendix C. As we have seen before, the former shows that  
 436 anomalies are still present when performing the analysis directly on the  $\bar{\rho}_\mu$  data without any  
 437 reference to the muon LDF or the corresponding  $N_\mu$  correction function (see fig. 6). While  
 438 studies on Appendix C.4 have pointed out that the experimental uncertainties on the shape  
 439 of the muon LDF have not a leading effect on the observed  $\Lambda_\mu$  deviations. The tests however  
 440 did not deal with the muon LECF.

441 The muon LECF correlates the energy losses by all particles in the KASCADE shielded  
 442 stations with the number of crossing muons. Therefore, if the real contribution from elec-  
 443 trons, photons and hadrons is not well described by the models an important bias could  
 444 be introduced to the final estimations of the number of muons in measured EAS. Here,  
 445 we are confident, however, that the modeling is reliable at least for particles other than  
 446 muons. One of the reasons is that model independent studies performed in [13] have shown  
 447 the absence of systematic deviations between separate estimations of  $N_{ch}$  for vertical EAS  
 448 (where the contribution of muons is not dominant) with the KASCADE and the Grande  
 449 arrays, although they were obtained based on independent LECF's. And two further rea-  
 450 sons are that, as we will see at the end of this section, the measured  $\Lambda_{ch}$  parameter shows a  
 451 better agreement with the MC predictions and the attenuation length for shower electrons  
 452 obtained with Grande data seems to be in pretty good agreement with the one derived from  
 453 KASCADE measurements. Hence, the problem of the observed anomalies could rely in the  
 454 MC estimations of the energy deposits of the muons in the KASCADE penetrating detec-  
 455 tors at different radial distances to the EAS core and distinct zenith angles. If so, then a  
 456 lower/higher contribution per muon to the LECF of muons would be required at small/large  
 457 zenith angles in order to reduce the magnitude of the measured  $\Lambda_\mu$  and  $\alpha_\mu$  parameters and  
 458 to bring the data into agreement with the corresponding MC predictions. As a matter of  
 459 fact, this possibility is not in conflict with the general conclusion drawn at the beginning of

460 this section.

461 At the moment, for the following discussions, we will assume that the role of the muon  
462 LECF in the deviations is small as expected from the MC simulations and within this context  
463 we will explore some scenarios implied by the observed deviations.

464 *Possible interpretations of the observed anomaly.* One of the consequences of the mismatch  
465 between the observed and predicted  $\Lambda_\mu$  is that the measured muon shower size spectrum of  
466 cosmic rays attenuates more slowly with increasing atmospheric depth than the simulated  
467 spectra. This result could be interpreted in terms of an incorrect prediction of the muon  
468 content of vertical and inclined EAS by the high-energy hadronic interaction models. For  
469 example,  $N_\mu$  could be too large for inclined showers in MC simulations, or too low in case  
470 of vertical EAS.

471 There are several possible ways to modify the muon number of EAS in simulations in  
472 order to obtain a larger muon attenuation length. Some tests carried out with EPOS-LHC  
473 and QGSJET-II-04 seem to indicate that at KASCADE-Grande, for EAS below  $\theta = 40^\circ$ ,  
474 we are very close to the region of the maximum of the muon longitudinal profile. This  
475 implies that if the shower maximum is closer to the ground then  $\Lambda_\mu$ , as reconstructed with  
476 equation (3), will raise and even more will become more sensitive to the position of the  
477 shower maximum. That is a geometric effect that should hold for any hadronic interaction  
478 model (at least it was confirmed for EPOS-LHC and QGSJET-II-04 using EAS generated  
479 by light primaries). This way, under this situation, one way to increment the value of  $\Lambda_\mu$   
480 is by increasing the interaction depth of primary particles, because in this case the shower  
481 maximum would be even closer to the observation level [30]. A similar effect can be obtained  
482 by having air showers that penetrate deeper into the atmosphere [31]. The need for more  
483 penetrating air showers in simulations is a plausible situation, which seems to be supported  
484 by both the analysis of the muon production heights measured with the muon tracking  
485 detector (MTD) of the KASCADE observatory [32, 33] and the study of the flatness of the  
486  $\bar{\rho}_\mu(r)$  distributions measured with the KASCADE muon array (see Appendix C.4). The  
487 former has revealed that the maxima of the muon production height distributions occur at  
488 lower altitudes than in MC simulations, while the latter has shown that the measured muon  
489 LDF's are steeper than the ones obtained from the MC models. That  $\Lambda_\mu$  increases when  
490 the shower maximum is closer to the detector level might be verified at the KASCADE-  
491 Grande data from the studies performed in Appendix C.6. There, the variation of the muon  
492 attenuation length with the atmospheric ground pressure or, equivalently, the atmospheric  
493 depth was calculated. In particular, an increment of  $\Lambda_\mu$  of  $\sim 16\%$  seems to be observed in  
494 the KASCADE-Grande data when decreasing the ground pressure by  $\sim 8 \text{ g/cm}^2$ . Again, we  
495 should remark that this only works when the maximum of the muon longitudinal profile is  
496 close to the ground, which seems to be the case for the EAS measured at KASCADE-Grande.

497 Larger  $\Lambda_\mu$  values can also be achieved in simulations by requiring a harder energy spec-  
498 trum for shower muons at production site [23]. It is worth to notice that if muons have  
499 a harder spectrum and hence a larger attenuation length, then the maximum of the muon  
500 longitudinal profile will be closer to the ground. This will further increase the magnitude of  
501  $\Lambda_\mu$  if the maximum is already close to the observation level. Therefore, one of the factors

502 which could have a remarkable effect on  $\Lambda_\mu$  is the muon energy spectrum at production site.  
 503 Amongst the models analyzed in this work, QGSJET-II-04 and EPOS-LHC are the ones  
 504 with the hardest spectra of muons, respectively. This might be the reason why they predict  
 505 the largest muon attenuation lengths in comparison with the other models. There are two  
 506 possible ways to achieve a harder muon spectrum in MC simulations: by an increase in the  
 507 amount of high energy muons in the EAS or by a decrease in the number of low energy  
 508 muons in the shower<sup>10</sup>. In order to discriminate between these physical situations in the  
 509 present models an analysis of the muon data at different energy thresholds is compelling<sup>11</sup>.

510 In addition to the muon attenuation length, the  $\alpha_\mu(r)$  coefficients may also provide some  
 511 information about overall differences between the energy spectrum of muons from MC and  
 512 measured data. What we have seen in fig. 6 is a deviation, which seems to increase with the  
 513 radial distance  $r$  to the shower core (measured at the shower plane). This behavior might  
 514 point out important deficiencies of the hadronic interaction models in describing also the  
 515 correct proportion of low energy muons to high energy ones but as a function of the lateral  
 516 distance,  $r$ . At closer distances to the EAS core, fig. 6 seems to suggest that an increase in  
 517 the amount of high energy muons could be appropriate at least for QGSJET-II-04 in order  
 518 to reproduce the experimental data on  $\alpha_\mu(r)$ , since the contribution of high energy muons  
 519 to the LDF's becomes more important close to the shower axis [5, 35, 36].

520 On the other hand, at larger distances from the EAS core, where low energy muons are  
 521 more important, the aforesaid figure seems to indicate that modifications are necessary for all  
 522 the studied models. In this case, the observed deviations might call not only for a reduction  
 523 in the amount of low energy muons in the simulated EAS, but also for an increment in the  
 524 content of muons at higher energies. The latter in view of the fact that as the zenith-angle  
 525 increases, both the experimental energy threshold and the mean energy of the muons rise  
 526 [30]. This way, the muon content in inclined showers becomes more sensitive to the high  
 527 energy part of the spectrum, which can lead to a rise in the value of  $\alpha_\mu(r)$  at large distances  
 528 from the core if the number of high energy muons is increased.

529 *Role of the low-energy hadronic interaction models.* We are assigning the discrepancy be-  
 530 tween the measurements and the simulations to the influence of the high-energy hadronic  
 531 interaction models. But, as we measure muons with a 230 MeV energy threshold at sea  
 532 level, both the muon number of EAS and the lateral density of muons are affected by the  
 533 decay products of low energy charged mesons from the last part of the shower development  
 534 [35, 37, 38]. Thus, a change in the description of the low-energy hadronic interactions might  
 535 also have important modifications to the magnitudes of  $\alpha_\mu(r)$  and  $\Lambda_\mu$ , mainly at large dis-  
 536 tances from the core. Therefore, low-energy hadronic interaction models might be playing

---

<sup>10</sup>In both cases the discrepancy would depend also on the atmospheric grammage decreasing at altitudes closer to the height where the maximum number of shower muons is reached.

<sup>11</sup>Fortunately, such analysis can be performed at KASCADE-Grande using the surface muon array, the underground muon tracking detector (MTD) and/or the tracking chambers from the central detector [34]. Since such analysis is underway, further hints to check the deficiencies of the models concerning the energy spectrum of muons may be obtained in the future.

537 a relevant role in the discrepancy. The issue will be investigated in detail in forthcoming  
538 studies.

539 *Consequences of the  $\Lambda_\mu$  anomaly.* Due to the rapid attenuation of the simulated data in  
540 comparison with the actual one, the discrepancy has some implications for the energy spec-  
541 trum and the composition studies of cosmic rays when air-shower data from different zenith  
542 angles are employed. In the first case, the anomaly will introduce a shift to higher energies on  
543 the primary spectra of cosmic rays reconstructed with  $N_\mu$  data from inclined showers. This  
544 shift was observed in the analysis of [21], where it was shown that, for measured EAS with  
545  $\theta < 40^\circ$ , the anomaly introduces an uncertainty of 6.5% at  $10^{16}$  eV and 10.9% at  $10^{17}$  eV in  
546 the respective all-particle cosmic ray flux when using QGSJET II-02 as a framework for the  
547 energy calibration of the data.

548 As a consequence of the above shift, the elemental composition of cosmic rays as inferred  
549 from the measured data using the high-energy hadronic interaction models appears heavier  
550 with increasing zenith angles. Indeed, inside the framework of the discussed hadronic inter-  
551 action models, the analyses of the muon densities at different  $N_{ch}^{CIC}$  bins and zenith-angle  
552 intervals (c.f. fig. 7) show that the actual  $\bar{\rho}_\mu(r)$  distributions move gradually towards a heav-  
553 ier composition for inclined showers. As an example, EPOS-LHC favors a light composition  
554 at around  $10^{17}$  eV for vertical EAS, while for inclined showers the model indicates that a  
555 mixed composition is dominant in the experimental data at roughly the same energy.

556 The source of disagreement between the measured and the predicted  $\Lambda_\mu$  in KASCADE-  
557 Grande could be also responsible for another anomaly detected at higher energies by the  
558 Pierre Auger collaboration. Measurements performed with the Auger observatory have  
559 shown an excess of the total  $\mu$ -content ( $E_\mu > 0.3$  GeV) in experimental data at ultra-high  
560 energies in comparison with expectations from modern MC simulations. Such anomaly has  
561 been observed also with the Yakutsk array ( $E_\mu > 1$  GeV) [39]. The discrepancy seems  
562 to be energy [7] and zenith-angle dependent [40] and can not be described by any of the  
563 available hadronic interaction models. Remarkably the largest deviations observed with the  
564 Auger detector between MC predictions and experimental data seems to occur for inclined  
565 showers and the highest energies. The latter might imply that model predictions can not  
566 even match the muon attenuation length of EAS at ultra-high energies and that such effect  
567 could evolve with the shower energy. A possible energy dependence of the  $\Lambda_\mu$  anomaly will  
568 be investigated in future studies at KASCADE-Grande by adding EAS data with shower  
569 energies below  $10^{16}$  eV from the KASCADE array.

570 With the aim of having a better understanding of the muon deviation measured at the  
571 KASCADE-Grande detector, independent studies from other observatories on the matter  
572 could be useful, specifically, at the energy range explored in this paper, using the current MC  
573 models. Unfortunately, such studies are absent at the moment. Muon data exists around  
574  $E = 10^{17}$  eV from HiRes-MIA ( $E_\mu > 850$  MeV) [41], the EAS-MSU array ( $E_\mu > 10$  GeV)  
575 [42] and the IceTop ( $E_\mu > 200$  MeV) experiment [43], but the analyses have been restricted  
576 only to look for a possible muon excess in the measured data over model predictions in a  
577 zenith-angle independent way. Hence, it is not possible to say whether the  $\Lambda_\mu$  anomalies are  
578 also present at the experimental conditions (i.e., muon energy thresholds, radial ranges and

579 air grammages) of such observatories. Undoubtedly these information would help to provide  
580 a wider picture of the above problem and narrow down the number of possible solutions.

581 *Remarks about  $\Lambda_{ch}$ .* Regarding our results corresponding to the attenuation length of  $N_{ch}$   
582 (see Appendix D), we see a better agreement between the experiment and the MC sim-  
583 ulations than in the case of  $\Lambda_{\mu}$ . In fact, the deviations of the measured  $\Lambda_{ch}$  from model  
584 predictions are less than  $+1.39\sigma$ . By comparing the results obtained with the QGSJET-  
585 II models, we observe that the post-LHC improvements performed in the last version of  
586 QGSJET-II did not spoil the agreement between the predicted and measured values of  $\Lambda_{ch}$ .  
587 That is an important constraint that, among other ones (such as the electron-muon corre-  
588 lations [44]) must be supervised when applying modifications to the models.

589 Since, at the energies and zenith angles involved in the analysis,  $N_{ch}$  is dominated by  
590 shower electrons, the fact that the value of  $\Lambda_{ch}$  is closer to the predictions of the models  
591 might indicate that the cause of the anomaly observed in the longitudinal development  
592 of  $N_{\mu}$  in the atmosphere has not a strong impact on the atmospheric attenuation of the  
593 electromagnetic component of the EAS.

594 We observed that the magnitude of  $\Lambda_{ch}$  is smaller than  $\Lambda_{\mu}$ . This is expected due to  
595 the stronger attenuation of  $N_e$  in comparison with  $N_{\mu}$  and the dominance of electrons over  
596 muons in  $N_{ch}$  for our selected data set. Following the same reasoning, we should also expect  
597  $\Lambda_{ch}$  to be closer to the attenuation length for the number of electrons,  $\Lambda_e$ . In order to verify  
598 the consistency of the results, we calculated  $\Lambda_e$  and compared it with  $\Lambda_{ch}$ . By applying the  
599 CIC method to the experimental data on  $N_e$ , we obtained  $\Lambda_e = 192 \pm 8 \text{ g/cm}^2$  from fits to  
600 the data in the interval  $\log_{10} N_e = [5.9, 7.1]$  (only the error from the global fit is quoted)<sup>12</sup>.  
601 This value is just  $1.1\sigma$  below  $\Lambda_{ch}$ . Therefore, in light of the previous discussions, we found  
602 that, inside the corresponding experimental uncertainties, the measurements of  $\Lambda_{ch}$  and  $\Lambda_e$   
603 are not inconsistent between each other.

## 604 7. Implications for the features of hadronic interaction models

605 The physical origin of the  $\Lambda_{\mu}$  discrepancy is not yet clear. Insofar, as the attenuation of  
606 muons in matter is concerned, this process is almost completely described by QED (with the  
607 exception of deep inelastic scattering, which contributes to the energy loss only less than 1  
608 %). Assuming that electromagnetic processes in air showers are well described by the EGS4  
609 [45] code used in COSIKA, any inconsistency between the measured and predicted muon  
610 attenuation lengths must be attributed to the modeling of hadronic interactions or to the  
611 description of the hadronic shower development in the atmosphere. This way, our results  
612 would indicate that the high-energy hadronic interaction models QGSJET-II-02, SIBYLL  
613 2.1, EPOS-LHC and QGSJET-II-04 need modifications to resolve the discrepancy with the  
614 muon data from KASCADE-Grande.

---

<sup>12</sup>The result is in full agreement with the measurements performed with KASCADE at lower energies. In this case,  $\Lambda_e$  was found to vary between 170 and 192 g/cm<sup>2</sup> using the CIC method in the interval 4.5 – 6.5 of  $\log_{10}(N_e)$  [48].

615 In the last section we discussed some possible modifications of EAS characteristics in  
616 the models, which might help to solve the muon attenuation length problem observed at  
617 KASCADE-Grande, e.g., an increase in the depth of the first hadronic interaction in the  
618 EAS, a deeper muon production height and a harder muon energy spectrum at production  
619 site. Now, we will discuss some changes of the characteristics of the internal parameters of  
620 the high-energy hadronic interaction models that might produce the variations in the EAS  
621 observables desired to explain the  $\Lambda_\mu$  anomaly.

622 In order to change the depth of the first interaction of the incident cosmic ray,  $X_1$ , the  
623 relevant parameter is the cross section for inelastic collisions with air,  $\sigma_I$ . Since,  $X_1 \propto 1/\sigma_I$   
624 [24], the depth of the first interaction can be increased by reducing  $\sigma_I$ . However, in this  
625 regard, there is not much room left due to the strong constraints set on the models by the  
626 LHC proton-proton data [46, 47]. Consequently, this possibility might just have a minor  
627 contribution to the discrepancy after all.

628 A bigger effect could be obtained from a deeper muon production depth (MPD) in the  
629 atmosphere,  $X^\mu$ . The latter can be achieved by modifying the description of pion-nucleus  
630 interactions, which is an important source of uncertainty in the models. More specifically,  
631 from detailed studies performed in [49, 50],  $X^\mu$  can be augmented principally through an  
632 increase of pion elasticity, a smaller pion-air inelastic cross section, harder secondary hadron  
633 spectra in pion-air collisions and/or a copious production of (anti-)baryons. The last option,  
634 however, it is not useful to enlarge  $\Lambda_\mu$  as we will explain later, therefore it might be discarded  
635 as a possibility to reduce the anomaly. The remaining options, on the other hand, could be  
636 coherent with an increase of  $\Lambda_\mu$ . Here, special care must be taken to be consistent also with  
637 the Pierre Auger measurements on the average value of  $X_{max}^\mu$ , i.e. the maximum of the  $X^\mu$   
638 profile [6]. In case of EPOS-LHC, for example, a further increase of  $X^\mu$  is not supported  
639 by the Auger data. The reason is that the respective model predictions are well above the  
640 experimental values at ultra-high energies. In this case a reduction of  $X^\mu$  is imperative.  
641 This can be achieved, for example, through a decrease of the elasticity in pion interactions  
642 [23] and/or a suppression of forward production of baryon-antibaryon pairs [50]. The first  
643 change could lead to an opposite effect in  $\Lambda_\mu$  to the one desired, while the second one could  
644 be coherent with the intended objective.

645 Of great importance for the problem could be the hadron and resonant production pro-  
646 cesses that keep energy of the shower in the hadronic channel and which could be misrep-  
647 resented in the models. They can modify the expected energy spectra of muons and, hence, the  
648 predicted muon attenuation lengths. To this category belongs the creation of (anti-)baryons  
649 in pion-air interactions. It is known that the abundant production of baryon-antibaryon  
650 pairs enhances  $N_\mu$  [51, 52], but it also increases the proportion of low energy muons in the  
651 shower. Thus, if it is overestimated, it might shorten the muon attenuation length and,  
652 hence, it could increase the  $\Lambda_\mu$  discrepancy. That seems to be happening in EPOS-LHC  
653 as it is suggested by Auger data on  $X_{max}^\mu$ . In principle, solving the problem of low energy  
654 muons in EPOS-LHC will put  $X_{max}^\mu$  higher in the atmosphere in agreement with the Auger  
655 observations, but it will also produce a harder muon energy spectrum and hence an increase  
656 of the distance between the MPD (where the muons are created) and the maximum of the  
657 muon longitudinal profile putting the latter closer to the ground, which is an important

658 factor to increase  $\Lambda_\mu$ .

659 A further mechanism that changes the muon energy spectra of EAS and is not well  
660 described in some models is the production of  $\rho^0$  resonances in pion-nucleus interactions.  
661 This process could also prove to be valuable to reduce the proportion of low energy muons at  
662 ground and to increase the magnitude of  $\Lambda_\mu$  in the models. The reason is that this mechanism  
663 enhances the production of high energy muons during the early stages of the EAS. After  
664 production, the  $\rho^0$  mesons decay almost immediately into a pair of charged pions [52]. At  
665 the early stages of shower development, these pions have a bigger probability to decay  
666 than to interact in the air (because the density of the atmosphere is low at high altitudes)  
667 resulting in the creation of high energy muons [53]. In particular, QGSJET-II-02, SIBYLL  
668 2.1 and EPOS-LHC underestimate the fixed-target experimental results on the very forward  
669 spectrum of  $\rho^0$ -mesons in pion-nucleus interactions [54]. Consequently, an enhancement of  
670 the above mechanism in these high-energy hadronic interaction models is necessary. This  
671 improvement might decrease the  $\Lambda_\mu$  differences between models and experiment in these  
672 cases.

673 The transverse momentum ( $p_t$ ) distributions of charged pions generated in pion-nucleus  
674 collisions may also need further tuning inside the current high-energy hadronic interaction  
675 models, as revealed by the results of the NA61/SHINE experiment about the spectra of  
676 charged pions in  $\pi^- - C$  interactions [54]. The  $p_t$  distributions of  $\pi^\pm$ 's have a relevant  
677 influence on the muon LDF's. Hence, it seems plausible that they would have also some  
678 impact on the magnitude of  $\Lambda_\mu$  as extracted from the local measurements of muons in EAS  
679 at KASCADE-Grande.

680 Finally, one could question the role of the approximations implemented in EGS4 [45]  
681 in the  $\Lambda_\mu$  discrepancy. This is an open issue, which has not been fully investigated. One  
682 might argue, therefore, that the observed anomaly could receive some contributions from an  
683 inaccurate description of the electromagnetic process behind both the attenuation of muons  
684 in the atmosphere or the photoproduction of low energy muon pairs. In spite of that, we  
685 might stress the role of the hadronic interaction models in the observed anomaly, as there  
686 are no direct experimental evidence for the existence of problems with such approximations  
687 which could give further support to the aforesaid hypothesis.

## 688 8. Conclusions

689 In this paper, the QGSJET-II-02, SIBYLL 2.1, EPOS-LHC and QGSJET-II-04 high-  
690 energy hadronic interaction models have been tested by comparing their predictions for the  
691 attenuation length of muons in EAS with the measurements performed with the KASCADE-  
692 Grande experiment at the energy interval  $E \approx 10^{16.3} - 10^{17.0}$  eV. In particular, it was found  
693 that the experimental  $\Lambda_\mu$  value is above  $+2.04\sigma$  and  $+1.99\sigma$  from the QGSJET-II-02 and  
694 SIBYLL 2.1 expectations, respectively, and just  $+1.48\sigma$  and  $+1.34\sigma$  from the corresponding  
695 QGSJET-II-04 and EPOS-LHC predictions. The above implies that the studied pre-LHC  
696 models do not match the measured value of  $\Lambda_\mu$ , while the post-LHC models are in relatively  
697 good agreement with the data. Despite of the latter, however, the fact that the expected

698 muon attenuation lengths from the post-LHC models are below the actual value seems to  
699 suggest that these models need further tuning to describe the KASCADE-Grande data.

700 To investigate the possible origin of the above deviations, predictions for the average  
701 muon densities at different zenith angles and  $E \approx 10^{16.9} - 10^{17.2}$  eV along attenuation curves  
702 in shower size were also confronted with the experiment. In general, it was found that  
703 the measured absorption lengths of the aforesaid mean muon density distributions become  
704 bigger than the predictions of the high-energy hadronic interaction models analysed in this  
705 work at large distances from the EAS core. According to complementary tests performed  
706 with MC simulations, we found that the aforesaid discrepancies could be the cause of the  
707 observed differences between the measured and the expected  $\Lambda_\mu$  values.

708 Finally, the attenuation length of  $N_{ch}$  was also measured and compared with the pre-  
709 dictions of the hadronic interaction models. In this case, a better agreement between the  
710 experiment and expectations was observed with differences ranging from  $+0.51\sigma$  to  $+1.39\sigma$ .

711 In conclusion, the QGSJET-II-02, SIBYLL 2.1, EPOS-LHC and QGSJET-II-04 hadronic  
712 interaction models do not reproduce consistently the zenith-angle behavior of the selected  
713 KASCADE-Grande data on the local muon content (with threshold energies  $E_\mu \geq 230$  MeV  
714 at vertical incidence) of EAS.

## 715 Acknowledgments

716 The authors would like to thank the members of the engineering and technical staff of  
717 the KASCADE-Grande Collaboration, who contributed to the success of the experiment.  
718 The KASCADE-Grande experiment was supported in Germany by the BMBF and by the  
719 Helmholtz Alliance for Astroparticle Physics - HAP funded by the Initiative and Networking  
720 Fund of the Helmholtz Association, by the MIUR and INAF of Italy, the Polish Ministry of  
721 Science and Higher Education, the Romanian Authority for Scientific Research UEFISCDI  
722 (PNII-IDEI grants 271/2011 and 17/2011), and the German-Mexican bilateral collabora-  
723 tion grants (DAAD-CONACYT 2009-2012, 2015-2016). J.C.A.V. acknowledges the partial  
724 support of CONACyT (grant CB-2008/106717) and the Coordinación de la Investigación  
725 Científica de la Universidad Michoacana.

## 726 Appendix A. Muon Correction function

727 The location of the muon detectors at the fringe of the Grande array, the limited size of  
728 the muon array and the detection and reconstruction procedures introduce a systematic error  
729 on the muon size, which depends on the arrival angle, the core position and the shower size.  
730 In order to improve the accuracy of the EAS observable and eliminate, as much as possible,  
731 the influence of the muon systematic errors on the study, a muon correction function is  
732 applied. The correction is achieved by using a single function that is derived from MC data,  
733 in particular, the QGSJET-II-02 data set, which has a better statistics and hence a reduced  
734 statistical error. Herein the shape of the function is parameterized in terms of the shower  
735 core position at ground, the shower size and the EAS zenith and azimuth angles. In the  
736 derivation of the correction function, the mixed composition scenario is assumed obeying to

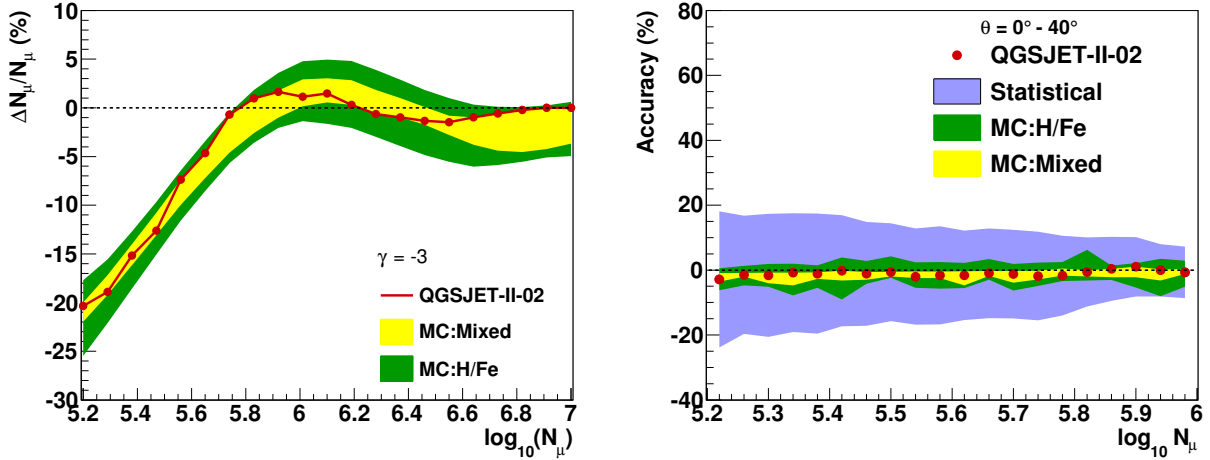


Figure A1: Left: Mean value of the muon correction function against the uncorrected  $N_\mu$  for different hadronic interaction models assuming a primary spectral index  $\gamma = -3$ . The function was evaluated for the KASCADE-Grande fiducial area and for a solid angle with  $\theta = [0^\circ, 40^\circ]$ . Right: Mean value of the systematic errors for the corrected muon number plotted as a function of the corrected  $N_\mu$ . In both figures, the points represent the results for QGSJET-II-02 assuming mixed composition. The error band in yellow labeled by *mixed* covers the range of variation of the results when a mixed composition scenario is assumed and the different hadronic interaction models studied in this paper are individually employed: QGSJET-II-02, SIBYLL 2.1, EPOS-LHC and QGSJET-II-04. On the other hand, the green band covers the expectations for pure hydrogen and iron nuclei. Finally, the gray band that appears on the right figure is the statistical error band for the results of QGSJET-II-02 shown with points.

737 the uncertainty of the elemental abundances in cosmic rays. Also a spectral index  $\gamma = -3$   
738 is employed.

739 The use of a single correction function on the muon data is justified since it is nearly  
740 independent of the composition and the hadronic interaction models explored here. Using  
741 other hadronic models and/or different composition assumptions just introduces small rela-  
742 tive differences (within  $\approx \pm 5\%$ ) in the correction function. This can be appreciated in fig. A1  
743 (left), where the mean value of the muon correction function from QGSJET-II-02 is plotted  
744 against the uncorrected  $N_\mu$  for showers with cores inside the KASCADE-Grande fiducial  
745 area and EAS axes between  $\theta = 0^\circ$  and  $40^\circ$ . The plots are shown along with two error bands  
746 that cover the range of results for alternative correction functions derived individually from  
747 different hadronic interaction models and composition scenarios. In fig. A1, we observe that  
748 for EAS with low  $N_\mu$ , the correction on the reconstructed muon number is large. That is  
749 because for low energy events located outside the KASCADE detector area the number of  
750 muons is overestimated. The reason is well known and it is due to the fact that the LDF  
751 that is used to get  $N_\mu$  on an event-by-event basis is steeper than the measured distribution  
752 of local muon densities for the EAS with the abovementioned characteristics [13]. At high  
753 energies, this difference decreases, which reduce the uncertainty of the reconstructed  $N_\mu$  and  
754 thus the magnitude of the applied muon correction as observed in fig. A1.

755 The mean systematic errors of the corrected muon number are displayed in fig. A1 (right)

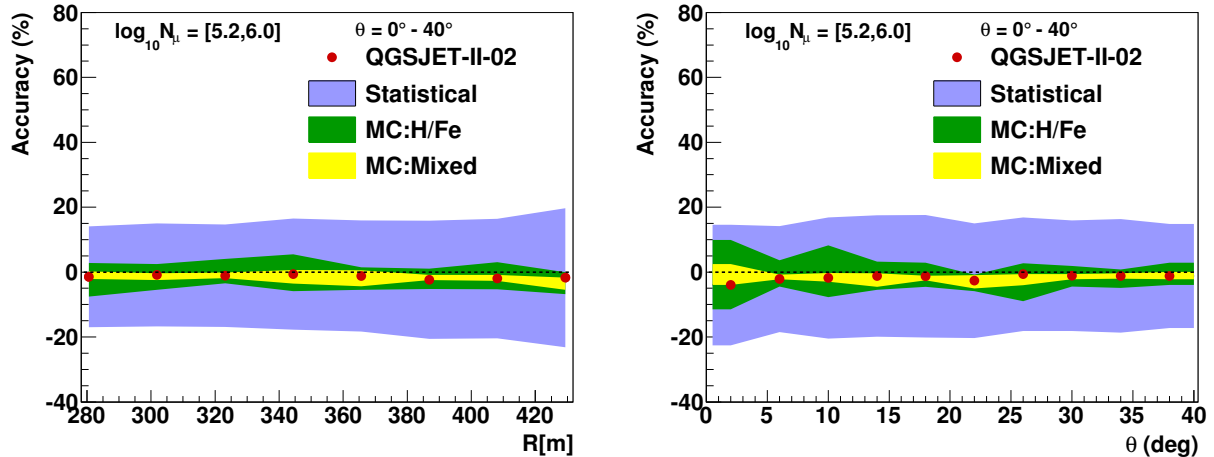


Figure A2: Mean value of the systematic uncertainties for the corrected muon number expected for the fiducial area of KASCADE-Grande and the zenith-angle interval  $\theta = [0^\circ, 40^\circ]$ . Errors are presented for corrected muon numbers within the interval  $\log_{10} N_\mu = [5.2, 6.0]$ , where the analysis of  $\Lambda_\mu$  was performed. The systematic errors are shown as a function of the core distance to the KASCADE center (left) and the shower zenith angle (right). In both figures, the points represent the results for QGSJET-II-02 assuming mixed composition. The meaning of the yellow, green and gray bands is the same as in fig. A1.

756 and fig. A2 as a function of the the muon size, the core position and the shower zenith angle  
757 in the full efficiency and maximum statistics regime. We can see that the final systematic  
758 errors are less than 10%. Although, this remaining bias is small we have not neglected it and  
759 have considered it in the evaluation of the final uncertainties of the muon attenuation length.  
760

## 761 Appendix B. Error estimation on $\Lambda_\mu$

762 In table B1 the total uncertainties for  $\Lambda_\mu$  are shown with the individual contributions  
763 from statistical and systematic errors. For the case of MC simulations the total errors vary  
764 in the range from  $\approx -30\%$  to  $\approx +28\%$ , while for experimental data they are found to  
765 be between  $-20\%$  and  $+19\%$ . In the following, we will list both the main statistical and  
766 systematic uncertainties that we have taken into account in the above estimations and briefly  
767 describe how they were calculated.

768 *Statistical error.* For the estimation of the influence of statistical fluctuations on the  
769 measured  $\Lambda_\mu$ ,  $\Phi_\mu$  intensities are randomly drawn from the original KASCADE-Grande muon  
770 shower size spectra by allowing the number of events per  $N_\mu$  interval and angular bin to  
771 fluctuate according to a Poisson distribution. For each trial, the integral intensities are  
772 then calculated from the drawn  $\Phi_\mu$  spectra for each zenith-angle interval according to eq. 2.  
773 Afterwards, the attenuation length is estimated with the usual method. The statistical  
774 error is therefore computed from the observed variability of  $\Lambda_\mu$  after 50 trials. In case of  
775 MC simulations, the procedure is similar, but with a single difference: as the MC data  
776 are weighted we use the formalism of the equivalent number of unweighted events [55] in

Table B1: Systematic and statistical uncertainties on the predicted and experimental muon attenuation lengths. Contributions to the global systematic error are also listed individually.

	QGSJET-II-02	QGSJET-II-04	SIBYLL 2.1	EPOS-LHC	KG data
<b>Statistical error (%)</b>					
Statistical fluctuations	$\pm 4.29$	$\pm 8.51$	$\pm 7.51$	$\pm 4.50$	$\pm 6.74$
<b>Systematics (%)</b>					
Muon systematics	+0.04	-2.30	-4.78	-2.53	+13.55/ - 10.60
Core far from KASCADE ( $R = [360, 440]$ m)	+2.37	-0.11	+2.57	+5.03	+11.89
Core close to KASCADE ( $R = [270, 360]$ m)	-3.38	+0.93	-5.90	-5.15	-10.73
Bin size	+6.14	+3.70	-2.05	+0.29	+6.79
Global fit	$\pm 4.96$	$\pm 5.40$	$\pm 5.39$	$\pm 5.05$	$\pm 5.60$
Muon Correction function uncertainties	+1.34	-1.11	+0.78	-2.25	-2.54
Broader zenith-angle interval (Four angular bins)	+1.61	-1.94	-1.21	+1.17	-2.42
Number CIC cuts	+1.12/ - 0.59	+2.29/ - 0.92	+0.38/ - 0.30	+0.11/ - 2.06	+1.40
Narrower CIC interval ( $\log_{10} N_\mu \approx [5.4, 6.0]$ )	-0.28	-2.90	-2.95	+2.88	-0.61
Spectral index uncertainties ( $\Delta\gamma = \pm 0.2$ )	+1.24/ - 0.62	+2.59/ - 0.71	+1.96/ - 3.26	-1.22	-
Composition	+10.91/ - 9.19	+25.96/ - 27.57	+0.07/ - 7.88	+18.98/ - 10.76	-
<b>Total (%)</b>					
	+14.57	+28.32	+9.84	+21.01	+19.46
	-11.82	-29.70	-15.18	-14.32	-19.71

777 the construction of the trial spectra, which allow us to properly evaluate the influence of  
778 statistical uncertainties on the expected  $\Lambda_\mu$  values.

779 Let  $N$  be the number of simulated events in a given  $N_\mu$ -bin and  $w_j$ , the individual  
780 weights of such events, where  $j = 1, \dots, N$ . Then the number of events in the corresponding  
781 bin of the weighted histogram is  $N^{ev} = \sum_{j=1}^N w_j$ , with  $\sigma(N^{ev}) = \sqrt{\sum_{j=1}^N w_j^2}$ , the respective  
782 statistical error. In general,  $N^{ev}$  does not follow a Poisson distribution, therefore, we replaced  
783 it by the equivalent number of unweighted events  $\tilde{N}^{ev} = (N^{ev})^2 / [\sigma(N^{ev})]^2$ . This quantity  
784 is Poisson distributed and has the same relative statistical uncertainty as  $N^{ev}$ . From here,  
785 we obtain the trial  $\Phi_\mu$  spectra that we require by allowing  $\tilde{N}^{ev}$  to fluctuate in each  $N_\mu$ -bin  
786 according to a Poisson distribution and after multiplying the result with a corresponding  
787 factor  $w_r = N^{ev} / \tilde{N}^{ev}$  to properly normalize the content of the bin.

788 *Error from the remaining systematic bias of the corrected muon number.* Its contribu-  
789 tion to the total error is obtained by propagating the uncertainties of the corrected  $N_\mu$   
790 to the differential spectra and then to the integral spectra employed in the derivation of the  
791 attenuation length. The systematic biases of the corrected  $N_\mu$  were estimated from MC  
792 data (see, for example, figs. A1 and A2). In case of simulations, they were applied in corre-  
793 spondence with the composition scenario and the hadronic model under study. In contrast,  
794 for measured data, all  $N_\mu$  systematic biases that are predicted by the hadronic models for  
795 several composition scenarios (i.e. five pure primary nuclei, from H to Fe, and a mixed com-  
796 position assumption) were used. We then compared the biases introduced in the measured  
797 muon attenuation length by these different hypotheses. The highest and lowest deviations  
798 are quoted as the errors of the measured  $\Lambda_\mu$  from the uncertainties of the corrected muon

799 number. We proceeded in this way due to the lack of knowledge of the actual systematic  
800 bias of the observed  $N_\mu$ , the real hadronic interaction model and the primary composition  
801 of cosmic rays. As a matter of fact, this is the reason why the contribution of the systematic  
802 bias of the corrected  $N_\mu$  is one of the biggest ones to the total experimental error. For MC  
803 simulations, on the other hand, this contribution was found to be small. The latter due to  
804 the fact that both the composition and the model are known.

805 *Influence of the EAS core position in the systematic uncertainty of  $\Lambda_\mu$ .* The contribution  
806 of this systematic source was investigated by dividing the central area into two smaller  
807 regions with approximately the same statistics. The division was done by applying a radial  
808 cut around 360 m from the center of the KASCADE array. To estimate the systematic  
809 errors, the muon attenuation lengths from the data collected on each surface were calculated  
810 independently and were later compared with the standard result for the whole area. The  
811 two differences obtained in this way were then cited independently as the errors due to the  
812 EAS core position. Using this analysis, we found a dependence of the measured attenuation  
813 length on the radial distance to the KASCADE center (see table B1), which is the origin  
814 of a major contribution to the total experimental uncertainty. By performing additional  
815 studies, we arrive at the result that the aforesaid EAS core dependence is due to a small  
816 decrease of the estimated number of muons, which is more important for vertical showers, as  
817 we move far away from the center of the KASCADE array. In MC data, this behaviour was  
818 not observed. In this case, the error analysis yielded just a mild dependence of the predicted  
819  $\Lambda_\mu$  with the EAS core position.

820 *Uncertainty from the CIC method.* This contribution covers the propagation of errors  
821 arising from the global fit and the variation of the results with the size of the zenith-angle  
822 intervals (studied by dividing the full zenith-angle range in four  $\theta$  intervals with the same  
823 aperture), the number of CIC cuts applied (using seven and three cuts instead of five), the  
824 width of the CIC interval (employing a narrower muon range for the fit:  $\log_{10} N_\mu \approx [5.4, 6.0]$ )  
825 and the size of the  $N_\mu$ -bins. The total experimental error arising from the uncertainties in  
826 the CIC method is found roughly between  $-6\%$  and  $+9\%$ , while the corresponding MC  
827 error lies between  $\approx -7\%$  and  $\approx +8\%$ . As we can see, both contributions are almost of  
828 the same order of magnitude and constitute also an important source of uncertainty in the  
829 estimation of the measured and predicted muon attenuation lengths, respectively.

830 *Errors of the parameters of the muon correction function.* To evaluate the influence of  
831 this contribution on the final  $\Lambda_\mu$  results, we propagated the errors in the determination of  
832 the parameters of the correction function (obtained under a mixed composition assumption  
833 with the QGSJET-II-02 model) to the  $N_\mu$  data and hence to the muon attenuation lengths.  
834 From table B1, we observe that the resulting shifts in the predicted and measured  $\Lambda_\mu$  values  
835 are in both cases small. Therefore this systematic source is not dominant.

836 *Uncertainties in the spectral index of the primary cosmic ray spectrum.* Only the uncer-  
837 tainties of the MC based predictions take into account this source of systematic error, which  
838 is evaluated by using two different values for the spectral index:  $\gamma = -2.8$  and  $-3.2$ , in the  
839 simulated data. The range of variation found in the corresponding  $\Lambda_\mu$  results with respect to  
840 the standard value with  $\gamma = -3.0$  is quoted as the systematic error from this contribution.  
841 In general, it results that the uncertainty in the spectral index has no major influence on

842 the magnitude of  $\Lambda_\mu$  expected from the high-energy hadronic interaction models.

843 *Uncertainties in the primary composition.* Systematic uncertainties for MC predictions  
844 include also the spreading of values when pure primary cosmic ray composition scenarios are  
845 considered. For these estimations, we employed five distinct elemental primary nuclei: H,  
846 He, C, Si and Fe. On the other hand, in order to reduce the influence of possible statistical  
847 effects, we have increased, in each case, the size of the zenith-angle bins employed in the CIC  
848 method. For this purpose, we reduced the number of  $\theta$  intervals in the analysis. In particular,  
849 we employed four zenith-angle ranges, i.e.  $\theta = [0^\circ, 18.75^\circ], [18.75^\circ, 27.03^\circ], [27.03^\circ, 33.82^\circ]$   
850 and  $[33.82^\circ, 40^\circ]$ , all of them with approximately equal aperture. We then extracted  $\Lambda_\mu$   
851 using the standard procedure for each primary composition assumption. The biggest and  
852 smallest values of  $\Lambda_\mu$  derived in this way for each model were considered as the errors of  
853 the expected  $\Lambda_\mu$  associated with the cosmic ray composition uncertainty. As we can see  
854 from table B1, they constitute the major source of uncertainty in MC predictions. It is  
855 worth to point out that, for measured data, this source of systematic error is already taken  
856 into account. Specifically, it is considered when calculating the contribution to the total  
857 experimental uncertainty due to the systematic biases of the corrected  $N_\mu$  for each of the  
858 aforementioned primary nuclei.

## 859 **Appendix C. Further systematic checks**

860 In this part of the paper, we evaluate the influence of suspected sources of systematic  
861 errors that might be at work in this analysis.

862  
863 *Aging of the muon detectors* From the experimental point of view, one possibility is the  
864 natural aging of both the plastic scintillator detectors and the PMT's of the KASCADE  
865 muon detectors. To quantify this effect, the measured data was divided in three subsamples  
866 with effective observation times of approximately the same order of magnitude and ordered  
867 in time. For each subset of data, the muon attenuation length was estimated (table C1). No  
868 dependency of the measured  $\Lambda_\mu$  on the time is observed. All values for the three different  
869 periods are in very good agreement within their own errors and are in accordance with  
870 the mean value shown in table 1 for the whole measured data sample (considering only  
871 statistical uncertainties, deviations are between  $\approx -0.25\sigma$  and  $\approx +0.29\sigma$ ). In consequence,  
872 it can be concluded that the aging of the muon detectors is not responsible for the observed  
873 discrepancy between the measured and the predicted muon attenuation lengths.

### 874 *Appendix C.1. Evolution of the elemental abundances of cosmic rays*

875 As we know from detailed studies performed in [20, 56, 57], the chemical composition  
876 of cosmic rays in the energy interval analysed is changing from light to heavy. Therefore  
877 the actual event samples contain a wide range of early and late developing showers, which  
878 might lead to a significant increase of  $\Lambda_\mu$  in comparison to the results with a single or  
879 equal-abundance composition scenarios. To quantify the influence of this effect, we used a  
880 toy model for the elemental composition of cosmic rays between  $10^{16}$  and  $10^{18}$  eV following  
881 the results of [20, 56, 57]. The model included the spectral features observed in the light

Table C1:  $\Lambda_\mu$  measured for different KASCADE-Grande subsets of data corresponding to three distinct periods. Statistical and systematic errors are shown in order of appearance. The latter only contains the contribution from the global fit.

	Period	Effective time (s)	$\Lambda_\mu$ (g/cm <sup>2</sup> )
Sample 1	20/12/2003 – 07/11/2006	$3.3 \times 10^7$	$1233 \pm 115 \pm 89$
Sample 2	07/11/2006 – 11/04/2009	$5.2 \times 10^7$	$1295 \pm 105 \pm 85$
Sample 3	11/04/2009 – 31/10/2011	$3.9 \times 10^7$	$1219 \pm 120 \pm 89$

882 and heavy components. Using the data from QGSJET-II-02 along with this elemental  
883 abundances, we calculated  $\Lambda_\mu$ . The result was just 1.4% smaller than the one obtained  
884 for the mixed composition assumption based on equal abundances. Therefore, the changing  
885 elemental abundances of cosmic rays in the studied energy regime is not causing the observed  
886 anomaly.

887 *Appendix C.2. Fluctuations on the number of registered muons per station*

888 Another interesting possibility is the influence of fluctuations on the number of registered  
889 muons  $n_\mu$  per KASCADE detector. The number of muons collected by a muon station  
890 is in general small, therefore fluctuations may play an important role here. In addition,  
891 fluctuations from MC simulations for  $n_\mu$  might be different from the experimental ones. All  
892 these effects together may lead to a bias in the reconstructed  $N_\mu$  explaining the observed  $\Lambda_\mu$   
893 deviations. In order to find out whether fluctuations on  $n_\mu$  are responsible for the deviations,  
894 QGSJET-II-02 simulations were employed. First,  $\rho_\mu$  fluctuations were obtained from the  
895 distributions of the density of muons as a function of the distance to the core at the shower  
896 plane (see as an example, fig. C1). The muon densities,  $\rho_\mu(r)$ , were built event-by-event  
897 by dividing the EAS plane in concentric rings (20 m width each) and then by dividing, for  
898 each radial interval, the corresponding amount of detected muons by the sum of projected  
899 effective areas of the active detectors located in that particular bin.

900 Fluctuations were extracted from both, MC and experimental data for the different  
901 zenith-angle ranges and for several  $N_{ch}$  intervals, where  $N_{ch}$  was corrected for attenuation  
902 effects in the atmosphere using the CIC method. To separate the data, the charged number of  
903 particles was chosen instead of  $N_\mu$  because in the former both the observed resolution and the  
904 agreement between the corresponding measured attenuation length and the MC predictions  
905 are better. MC fluctuations were obtained only for proton and iron nuclei as primaries,  
906 respectively. For experimental data, fluctuations might be overestimated since they might  
907 contain contributions from different primary elements. Once fluctuations were calculated,  
908 they were applied with a simulation program event-by-event to the MC data sets to estimate  
909 the number of particles detected per KASCADE muon station per simulated shower under  
910 each of the above fluctuation scenarios. For a given MC event with true muon content  
911  $N_\mu$ , the number of muons hitting each KASCADE muon station is estimated according  
912 to the geometry of the station and the muon lateral distribution function of equation (1).  
913 For this estimation the true values of the shower core position and arrival direction are

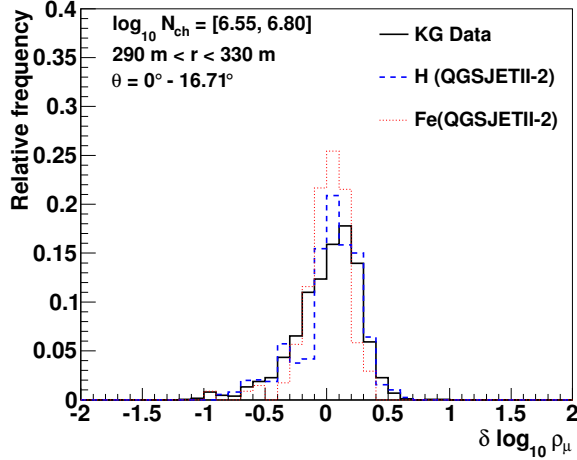


Figure C1: Measured distribution of the  $\rho_{\mu}$  fluctuations for a radial interval [290 m, 330 m] at the shower plane and for vertical showers in the range  $\log_{10} N_{ch} = [6.55, 6.80]$ , where  $N_{ch}$  has been corrected for attenuation effects in the atmosphere and normalized at  $\theta = 22^\circ$  with the CIC method. The distribution is compared with the predictions of QGSJET-II-02 for primary protons and iron nuclei.

914 needed. They are taken from the input parameters used in CORSIKA to simulate the  
 915 shower. Once the number of muons per station is known, this quantity is allowed to fluctuate  
 916 using the corresponding statistical distributions obtained from the experiment or simulated  
 917 data. Then, the new set of  $n_{\mu}$  values are stored and the mean deposited energy per muon  
 918 station is estimated. Henceforth, the standard KASCADE-Grande reconstruction software  
 919 is applied. The muon attenuation lengths are finally obtained from the reconstructed MC  
 920 data sets using the standard procedure described at the beginning of this section.

921 Interestingly, the final results with MC simulations showed that the  $\Lambda_{\mu}$  value obtained  
 922 with experimental fluctuations stays above the corresponding result derived when using  
 923 the MC ones, however the differences are small, just below 15% for QGSJET-II-02. In  
 924 consequence, the effect of the fluctuations on the number of muons per KASCADE muon  
 925 station can not explain the observed  $\Lambda_{\mu}$  discrepancy between measured and predicted data.

### 926 *Appendix C.3. Uncertainties of air shower parameters*

927 The influence of systematic errors coming from uncertainties in the reconstruction of the  
 928 core position, arrival direction and the number of muons per detector from the deposited  
 929 energy were also studied. For this purpose, new MC data sets were generated based on  
 930 QGSJET-II-02 and by using the true shower location, arrival direction and number of muons  
 931 hitting the KASCADE muon detectors in the reconstruction stage of the MC events. This  
 932 way, the  $N_{\mu}$  estimated for the resulting data sets has no influence from the systematic  
 933 errors due to mislocation of the core, misalignment of the reconstructed shower axis or  
 934 wrong estimation of  $n_{\mu}$  per station. For the new data sets, the  $\Lambda_{\mu}$  values are extracted  
 935 and are compared with the corresponding attenuation lengths from the data where the  
 936 uncertainties on the shower parameters are considered (for simplicity, in both cases, no  
 937 muon correction function was applied). From the comparison, it is concluded that the effect

938 of the abovementioned systematic errors on  $\Lambda_\mu$  is to modify its magnitude, but by a negligible  
 939 amount ( $\lesssim 3\%$ ).

940 These are conservative predictions associated with the effects of core and angular reso-  
 941 lutions. One can ask what would happen if the actual magnitude of systematic errors of the  
 942 core position and arrival direction were somewhat different. For this possibility there is not  
 943 much room left, since the resolution of the Grande detector has been checked out with the  
 944 KASCADE array, which works independently of the former as mentioned in section 2. By  
 945 introducing these errors [13] in our MC simulations the muon attenuation length varies just  
 946 within 7%. Therefore, in light of the above results, it is unlikely that systematic errors due  
 947 to shower core position and arrival direction could be the main cause for the  $\Lambda_\mu$  deviation  
 948 between experimental data and MC expectations.

#### 949 *Appendix C.4. Uncertainties of the muon LDF*

950 The fact that there is an intriguing dependence of the muon attenuation length on the  
 951 core position, which is not predicted by simulations, suggests the presence of another source  
 952 of systematic error of  $\Lambda_\mu$  (see Appendix B). One possibility could be found at the shape  
 953 of the muon lateral distribution function. During reconstruction the slope of the LDF is  
 954 kept constant due to the fact that the KASCADE muon detectors only sample a limited  
 955 portion of the EAS. However, it is known that, although the measured LDF for muons is  
 956 bracketed by simulation results, the observed slopes are different from MC predictions [58].  
 957 By comparing the slopes of the mean muon lateral distribution functions expected from MC  
 958 simulations and the ones observed in experimental data, we found that, on average, the  
 959 MC distributions are flatter than the measured ones. These differences clearly suggest the  
 960 presence of a potential source of systematic error of  $N_\mu$ , which may be also contributing to the  
 961 observed anomaly. To estimate the possible contribution from this effect to the systematic  
 962 error of  $\Lambda_\mu$ , first, for each zenith-angle interval and the  $\log N_{ch}^{GIC}$  range discussed in section  
 963 5, we fitted the QGSJET-II-02 and the experimental mean muon density distributions with  
 964 formula (1) but using  $p_1$  and  $N_\mu$  as free parameters. This was done in order to get an  
 965 estimation of the flatness of the muon density distributions and to quantify the differences  
 966 between the slopes of the experimental and the expected LDF's. The fits were performed  
 967 on the radial interval  $r > 160$  m. For MC, we applied the fits on the data sets for pure  
 968 elements and mixed composition. From the fitted values of  $p_1$ , it was found that, in general,  
 969 the actual mean muon radial density distributions are on average  $7\% \pm 15\%$  steeper than  
 970 the MC simulated ones.

971 To evaluate the effect of using a flatter muon LDF to fit our data, we considered the MC  
 972 data sets of QGSJET-II-02 for a mixed composition scenario and proceeded to reconstruct  
 973  $N_\mu$  event-by-event with a flatter muon LDF. The latter was performed by decreasing the  
 974 magnitude of  $p_1$  by 22% in the LDF formula employed for the standard EAS reconstruction,  
 975 see eq. (1). This percentual decrement corresponds to the upper limit of the  $1\sigma$  interval  
 976 found for the difference between the  $p_1$  values of the MC and measured muon LDF's. For  
 977 the above variation, we found that  $\Lambda_\mu$  is shifted by +6%. In addition, the dependence of  
 978  $\Lambda_\mu$  on the distance to the KASCADE muon cluster became larger than the one observed  
 979 in table B1 for QGSJET-II-02. In particular,  $\Lambda_\mu$  decreases by  $-7\%$  for events with cores

980 between  $R = 270$  m to 360 m, and increases by +6 % at farther distances ( $R = [360, 440]$  m).  
 981 If now the magnitude of the parameter  $p_1$  of formula (1) is increased by 22 %, in order to  
 982 have a steeper muon LDF as suggested by the measured data, then we observe that the  
 983 experimental  $\Lambda_\mu$  is reduced only by  $\approx 8$  % ( $\sim 99$  g/cm<sup>2</sup>), while the core dependence of  $\Lambda_\mu$   
 984 remains still high ( $\pm 9$  %). Therefore, we see that the systematic errors of  $\Lambda_\mu$  are not enough  
 985 to be the cause of the discrepancy.

986 To give a better estimation of the effect of the  $\Delta p_1$  differences between the measured and  
 987 the MC data and with the aim of confirming the conclusion of the previous analysis, we used  
 988 an alternative approach: we weighted the  $\rho_\mu(r)$  distributions of the QGSJET-II-02 events for  
 989 the mixed composition assumption to reproduce a steeper LDF in closer agreement with the  
 990 one observed from the measurements. Then we applied the standard KASCADE-Grande  
 991 reconstruction algorithm to the aforementioned MC events to obtain  $N_\mu$  from which we  
 992 calculated  $\Lambda_\mu$ . Finally, the latter is compared with the standard result obtained from the  
 993 unmodified data sets. The weight was applied by multiplying the number of events recorded  
 994 in each station by the factor  $(r/320 \text{ m})^{\Delta p_1}$ , where  $\Delta p_1 = p_1^{KG} - p_1^{MC}$  is the mean difference in  
 995  $p_1$  obtained from the study described in the previous paragraph. Since  $\Delta p_1 = -0.07 \pm 0.16$ ,  
 996 we used the lower limit of this interval for the estimation of the  $\Lambda_\mu$  systematic uncertainty.  
 997 The result was an increase of  $\approx +8$  % ( $\sim 57$  g/cm<sup>2</sup>), which is of the order of magnitude of  
 998 the systematic error already calculated in the aforementioned paragraph.

999 One may argue that the individual differences between the LDF's at different zenith-  
 1000 angles may be contributing in some way to the  $\Lambda_\mu$  systematics too. In general, we have  
 1001 observed that both the MC and measured mean muon radial density distributions become  
 1002 flatter as the zenith-angle increases. However, the slope of the measured LDF's decreases  
 1003 faster than that derived from MC simulations. To quantify the influence of these effects on  
 1004 the muon anomaly, first we modelled the above differences based on the observed  $\Delta p_1(\theta)$  as  
 1005 obtained for the interval  $\log N_{ch}^{CIC} = [7.04, 7.28]$ . The differences were derived by comparing  
 1006 the experimental data with the results from the QGSJET-II-02 model for a mixed compo-  
 1007 sition scenario and primary spectrum  $\propto E^{-3}$ . Then we weighted the muon LDF's from the  
 1008 QGSJET-II-02 data sets by using the factor  $(r/320 \text{ m})^{\Delta p_1(\theta)}$ , with  $\Delta p_1(\theta) = -0.138 + 0.143 \cdot \theta$ ,  
 1009 with  $\theta$  in radians. Finally, we reconstructed  $N_\mu$  event-by-event and obtained  $\Lambda_\mu$  by the usual  
 1010 procedure. The result was a shift of  $\sim +2$  % on the simulated  $\Lambda_\mu$ .

1011 In summary, we conclude that it is improbable that the uncertainty on the slope of the  
 1012 LDF is the main cause of the deviation on the muon attenuation length.

### 1013 *Appendix C.5. Influence of the muon correction function*

1014 The prime suspect behind the  $\Lambda_\mu$  anomaly is the muon correction function applied to  
 1015 the data. In general, the effect of this function on the estimated  $\Lambda_\mu$  is to shift its magnitude  
 1016 by +13 % / - 3 % for MC simulations and +17 % for experimental data with respect to the  
 1017 value extracted from the uncorrected  $N_\mu$ . It is observed that the amount of shift for the  
 1018 experimental value is bigger than that for MC estimations. However, it does not explain  
 1019 the discrepancy. In fact, a more detailed analysis based on the mean lateral muon densities  
 1020 (see section 5) revealed that the differences between the measured and expected muon at-  
 1021 tenuation lengths are not an artefact from the application of the muon correction function

1022 on the data. In particular, it was observed that they can be tracked down to differences  
 1023 between the experimental and predicted evolutions of the local mean muon densities in the  
 1024 shower front with the angle  $\theta$ . This asseveration can be probed by modifying in an artifi-  
 1025 cial way the zenith-angle evolution of the muon lateral distribution functions obtained from  
 1026 MC simulations. We have employed the same simulated MC data sets used to study the  
 1027 impact of the uncertainties in the slope of the muon LDF's on  $\Lambda_\mu$ , and we have multiplied  
 1028 the corresponding muon densities by the factor  $\left[ e^{X_0(1-\sec\theta)\cdot(1/\bar{\alpha}_\mu^{KG}-1/\bar{\alpha}_\mu^{MC})} \cdot (r/320\text{ m})^{\Delta p_1(\theta)} \right]$ .  
 1029 Here,  $\bar{\alpha}_\mu^{KG} = (1159 \pm 110) \text{ g/cm}^2$  is the average value of the muon absorption length for  
 1030 the experimental data in the radial interval  $r = [220\text{ m}, 380\text{ m}]$  and the shower size range  
 1031  $\log N_{ch}^{CIC} = [7.04, 7.28]$  (see fig. 6). On the other hand,  $\bar{\alpha}_\mu^{MC} = (821 \pm 28) \text{ g/cm}^2$  is the corre-  
 1032 sponding value for the QGSJET-II-02 based simulations (mixed composition data in fig. 6).  
 1033 After applying the full reconstruction procedure to the new simulated data, we found that  
 1034  $\Lambda_\mu^{MC} = (1116 \pm 184) \text{ g/cm}^2$ , which is in pretty good agreement with the measured value.

### 1035 *Appendix C.6. Fluctuations on the local values of atmospheric temperature and pressure*

1036 The influence of local variations of the air pressure and temperature on our results were  
 1037 investigated. At the site, the mean pressure at ground during the DAQ period used for  
 1038 our analysis was  $\bar{P} = 1003.0 \pm 8.5 \text{ mbar}$ , which is pretty close (within the experimental  
 1039 RMS variations) to the nominal value of  $\approx 1002.2 \text{ mbar}$  ( $P_0 = 1022 \text{ g/cm}^2$ ) used for the  
 1040 MC simulations. To evaluate the influence of this small difference in the measured  $\Lambda_\mu$ , data  
 1041 within a small interval  $\Delta P_0$  around  $P_0$  was chosen and the corresponding muon attenuation  
 1042 length was evaluated. In particular, we used  $\Delta P_0 = [998.3 \text{ mbar}, 1006 \text{ mbar}]$ . This range  
 1043 was selected in such a way that  $P_0$  coincides with the median of the pressure distribution  
 1044 for the corresponding interval. The result for  $\Lambda_\mu$  is shown in table C2. This value is just  
 1045  $0.008 \sigma$  (for statistical errors only) below that corresponding to the full experimental data  
 1046 set. Therefore, the difference between the values  $P_0$  in the interval selected and  $\bar{P}$  can not  
 1047 be the main cause of the  $\Lambda_\mu$  discrepancy.

1048 To go further, we investigated the effect of the tails of the  $P$  distribution. For this  
 1049 purpose, we considered two additional data sets: one with  $P > 1006 \text{ mbar}$  and another one  
 1050 with  $P < 998.3 \text{ mbar}$ , and we calculated  $\Lambda_\mu$  for each case. The extracted values are presented  
 1051 in table C2. They are within  $-0.4 \sigma$  and  $+0.9 \sigma$  (using only statistical uncertainties for the  
 1052 comparison), respectively, from the main result obtained for the whole KASCADE-Grande  
 1053 data set. The magnitude of these deviations can not explain the observed anomaly of the  
 1054 muon attenuation length. If the smallest value of  $\Lambda_\mu$  obtained from the present analysis  
 1055 with different  $P$  intervals is compared with the MC predictions of table 1, deviations from  
 1056  $+3.2 \sigma$  to  $+4.6 \sigma$  arise (employing only statistical errors).

1057 On the other hand, it is also worth mentioning that a possible hint for a dependence of  
 1058 the  $\Lambda_\mu$  discrepancy with the mean atmospheric pressure seems to be observed in the data  
 1059 (see table C2). In particular, the results seem to suggest that the disagreement between  
 1060 the measured and predicted  $\Lambda_\mu$  parameters grows when decreasing the mean value of  $P$ .  
 1061 The effect seems to be the result of an apparent reduction in the estimated number of  
 1062 muons at lower pressures, which is more important for vertical showers. For example, when

Table C2: Attenuation lengths for the muon number extracted from experimental data for different intervals of pressure,  $P$  (mbar), and temperature,  $T$  ( $^{\circ}C$ ), at the site. Statistical and systematic errors are shown in order of appearance. The latter only contains the contribution from the global fit.

Interval	Mean ( $P, T$ )	Effective time (s)	$\Lambda_{\mu}$ (g/cm $^2$ )
$P > 1006.0$	(1012.0 $\pm$ 4.4, 7.8 $\pm$ 7.7)	$5.24 \times 10^7$	1204 $\pm$ 104 $\pm$ 79
$P = [998.3, 1006.0]$	(1002.0 $\pm$ 2.1, 12.9 $\pm$ 7.5)	$5.24 \times 10^7$	1255 $\pm$ 99 $\pm$ 81
$P < 998.3$	(992.5 $\pm$ 5.5, 9.8 $\pm$ 7.4)	$3.43 \times 10^7$	1405 $\pm$ 139 $\pm$ 109
$T > 14.15$	(1002.0 $\pm$ 5.4, 19.4 $\pm$ 4.0)	$4.54 \times 10^7$	1249 $\pm$ 111 $\pm$ 84
$T = [6.45, 14.15]$	(1003.0 $\pm$ 8.2, 10.3 $\pm$ 2.2)	$4.69 \times 10^7$	1234 $\pm$ 124 $\pm$ 86
$T < 6.45$	(1005.0 $\pm$ 10.6, 1.5 $\pm$ 3.5)	$4.68 \times 10^7$	1310 $\pm$ 160 $\pm$ 88

1063 comparing the muon attenuation curves derived for the data sets with  $P < 998.3$  mbar and  
1064  $P > 1006$  mbar, respectively, at the same CIC cut:  $\log_{10}[J/(\text{m}^{-2} \cdot \text{s}^{-1} \cdot \text{sr}^{-1})] = -8.60$ , it  
1065 is observed that for showers closer to the zenith (first angular bin), the magnitude of  $N_{\mu}$   
1066 derived from the CIC method for the interval with highest  $P$  is  $\approx 4.5\%$  bigger than that  
1067 obtained for the interval of lowest atmospheric pressure, while for inclined showers (last  
1068 zenith-angle bin) the difference is negligible and it amounts to  $\approx 0.7\%$ . The interpretation  
1069 of the results given here is still tentative as the statistical errors for the subsamples of table  
1070 1 are not small.

1071 Regarding the influence of the local variations of temperature on  $\Lambda_{\mu}$ , we have found  
1072 that it is not significant. The temperature at the site was continuously monitored from the  
1073 top of a tower at 200m above the ground. From the records of the temperature during  
1074 the DAQ period of the analysed data, we found that the mean value of the temperature  
1075 was  $\bar{T} = 10.27^{\circ}C$  with a standard deviation of  $7.88^{\circ}C$ . To study the effect of the local  
1076 temperature variations on the muon attenuation length, we divided our data in three subsets  
1077 according to the following temperature intervals:  $T < 6.45^{\circ}C$ ,  $T = [6.45^{\circ}C, 14.15^{\circ}C]$  and  
1078  $T > 14.15^{\circ}C$ , each of them with approximately the same statistics. Then we applied our  
1079 standard analysis to find  $\Lambda_{\mu}$  in each case (table C2). The results show variations from  $-0.1\sigma$   
1080 to  $+0.3\sigma$  from the measured value reported in table 1 for the whole experimental data set  
1081 (comparisons were performed using only statistical uncertainties). Therefore, it is unlikely  
1082 that the variations in the local temperature could be the cause of the observed  $\Lambda_{\mu}$  anomaly.

#### 1083 Appendix D. The attenuation length for $N_{ch}$

1084 In order to complement the present study, a last check was performed, but on  $N_{ch}$ , which  
1085 includes the number of muons and electrons of the shower. In this check, the  $N_{ch}$  attenuation  
1086 length,  $\Lambda_{ch}$ , was estimated from the KASCADE-Grande measurements of air showers and  
1087 the result was compared with the predictions from the hadronic interaction models of section  
1088 3. The extraction procedure of  $\Lambda_{ch}$  was identical to the one employed with  $\Lambda_{\mu}$ , with the  
1089 only exception that no correction function was applied. The latter was not necessary for

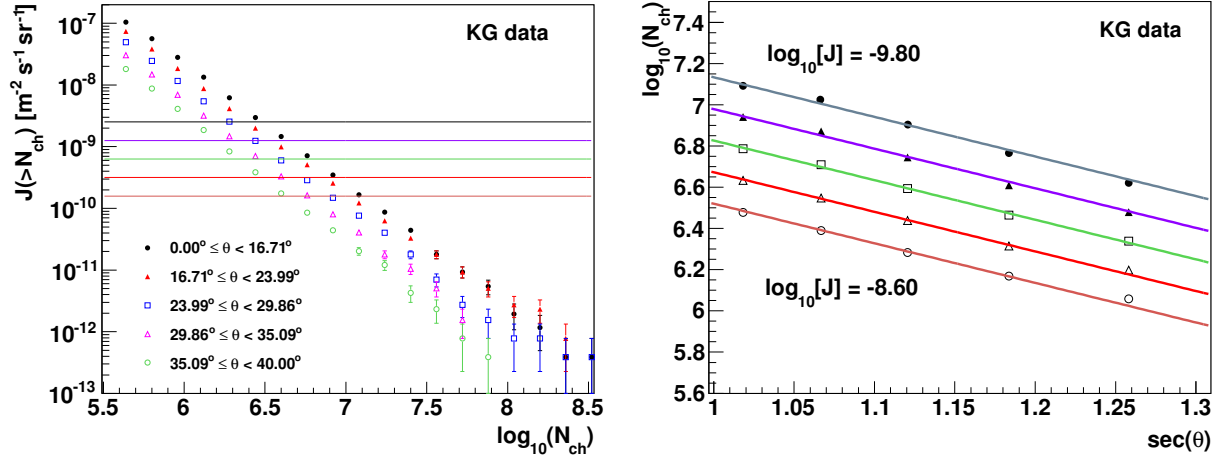


Figure D1: Left:  $N_{ch}$  integral spectra for five zenith-angle intervals derived from the measurements with the KASCADE-Grande observatory. Error bars represent statistical uncertainties. The CIC cuts employed in this work are shown as horizontal lines. Right:  $N_{ch}$  attenuation curves obtained by applying several constant intensity cuts to the KASCADE-Grande integral spectra,  $J_{ch}$ . The cuts decrease from the bottom to the top in units of  $\Delta \log_{10}[J/(\text{m}^{-2} \cdot \text{s}^{-1} \cdot \text{sr}^{-1})] = -0.30$ . Errors are smaller than the size of the symbols. They take into account statistical uncertainties, errors from interpolation as well as the correlation between adjacent points when interpolation was applied.

1090 the analysis, since in KASCADE-Grande the charged particle content of EAS is determined

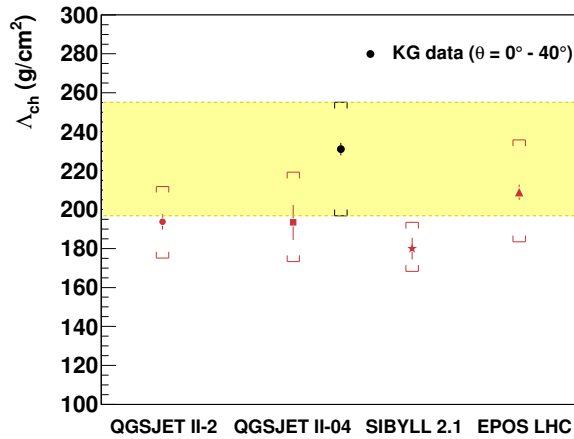


Figure D2:  $N_{ch}$  attenuation lengths extracted from Monte Carlo (lower red points) and experimental data (upper black circle). Error bars indicate statistical uncertainties, while the brackets represent the total errors (systematic plus statistical errors added in quadrature). The shadowed band covers the total uncertainty estimated for the experimental result.

Table D1: Attenuation lengths for the charged particle number extracted from Monte Carlo and experimental data.  $\Lambda_{ch}$  is presented along with their statistical and systematic errors (in order of appearance). Also the deviations (in units of  $\sigma$ ) of the measured  $\Lambda_{ch}$  from the predictions of different hadronic interaction models are shown. The one-tailed confidence levels (CL) that the measured value is in agreement with the MC predictions are also presented.

	QGSJET-II	QGSJET-II-04	SIBYLL 2.1	EPOS-LHC	KG data
$\Lambda_{ch}$ (g/cm <sup>2</sup> )	$194 \pm 4_{-18}^{+18}$	$193 \pm 9_{-18}^{+24}$	$180 \pm 6_{-10}^{+12}$	$209 \pm 4_{-25}^{+27}$	$231 \pm 3_{-34}^{+24}$
Deviation ( $\sigma$ )	+0.96	+0.88	+1.39	+0.51	
CL (%)	16.78	19.02	8.25	30.56	

1091 with a better precision than the muon number<sup>13</sup> [13].

1092 The measured  $N_{ch}$  integral spectra upon which the analysis is performed are presented  
1093 on the left side of fig. D1 along with the applied CIC cuts. On the right side of the same  
1094 figure, the  $N_{ch}$  attenuation curves extracted with the CIC method are also shown. As  
1095 before, the  $\Lambda_{ch}$  is obtained from a global fit with a relationship like (3) to the measured  
1096 attenuation curves. The resulting value is plotted on fig. D2 together with the predictions  
1097 from QGSJET-II-02, SIBYLL 2.1, QGSJET-II-04 and EPOS-LHC. The magnitudes of the  
1098 measured and predicted values of  $\Lambda_{ch}$  are displayed in table D1.

1099 To investigate the agreement between the measurement and the predictions from MC  
1100 simulations, a simple statistical analysis was applied. Deviations of the experimental  $\Lambda_{ch}$   
1101 from estimations of the models were computed and confidence levels for agreement with  
1102 the predictions of the hadronic interaction models were derived. The results are presented  
1103 in table D1. Herein a good consistency between experimental data and the predictions of  
1104 the high-energy hadronic interaction models can be seen, since the statistical analysis gives  
1105 deviations between  $+0.51\sigma$  and  $+1.39\sigma$ , with a CL from 8.25 % to 30.56 %, respectively,  
1106 which are as a matter of fact quite satisfactory.

1107 The total uncertainties of  $\Lambda_{ch}$  are presented in table D2 along with their corresponding  
1108 statistical and systematic errors. All of them were calculated in the same way that for  $\Lambda_{\mu}$ .  
1109 The results were found to vary in the range from  $\approx -15\%$  to  $\approx +13\%$ . In experimental  
1110 data, an important contribution to the total error of  $\Lambda_{ch}$  (between  $\approx -13\%$  and  $\approx +9\%$ )  
1111 is the systematic uncertainty of  $N_{ch}$ . The latter was estimated from MC simulations and  
1112 confirmed with experimental investigations [13]. On the other hand, in contrast to the  $\Lambda_{\mu}$   
1113 case, here no relevant dependence of the measured  $\Lambda_{ch}$  with the radial distance was found,  
1114 for the corresponding variations of  $\Lambda_{ch}$  were within  $\pm 2\%$  (see table D2). The reason is  
1115 that, for the charged component of EAS the LDF is well measured event-by-event across  
1116 the Grande detector area. Regarding MC simulations, a sizeable contribution in this case

<sup>13</sup>In turn, the number of electrons can be estimated even with a better precision than  $N_{ch}$  in KASCADE-Grande. For example, for our data set, after applying quality cuts, MC predictions indicate that for shower sizes  $\leq 3.2 \times 10^8$ , the systematics on  $N_e$  are  $\lesssim 7\%$ , while for  $N_{ch}$  are  $\lesssim 12\%$ .

Table D2: Total uncertainties on the predicted and experimental  $\Lambda_{ch}$ . The different contributions from the systematic and statistical errors are also shown.

	QGSJET-II	QGSJET-II-04	SIBYLL 2.1	EPOS-LHC	KG data
<b>Statistical error (%)</b>					
Statistical fluctuations	$\pm 2.05$	$\pm 4.65$	$\pm 3.10$	$\pm 1.89$	$\pm 1.38$
<b>Systematics (%)</b>					
Nch systematics	-1.90	-2.58	+0.94	-9.75	-13.55/ + 8.79
Global fit	$\pm 4.34$	$\pm 4.67$	$\pm 4.58$	$\pm 4.71$	$\pm 4.94$
Core far from KASCADE ( $R = [360, 440]$ m)	+2.26	-0.60	+0.54	+0.79	+2.04
Core close to KASCADE ( $R = [270, 360]$ m)	-2.91	-0.12	-1.99	-1.10	-2.07
Bin size	-1.90	+1.02	+2.81	-2.46	-1.59
Narrower CIC interval ( $\log_{10} N_{ch} \approx [6.1, 7.2]$ )	-0.75	-0.42	-0.73	+0.41	-1.49
Broader zenith-angle interval (Four angular bins)	+0.01	-0.33	+1.25	+0.28	-0.71
Number CIC cuts	-0.32/ + 0.23	-0.10/ + 0.09	-0.96/ + 0.27	-1.30/ + 0.20	-0.08/ + 0.47
Spectral index uncertainties $\Delta\gamma = \pm 0.2$	-1.11/ + 3.28	-0.44/ + 2.12	-0.56/ + 1.13	-1.89/ + 1.46	-
Composition	-7.18/ + 6.99	-7.61/ + 11.37	-2.36/ + 3.72	-3.98/ + 11.68	-
<b>Total</b>					
	+9.37	+13.35	+7.52	+12.86	+10.39
	-9.61	-10.43	-6.47	-12.22	-14.81

1117 came from the uncertain knowledge of the primary composition of the experimental sample.  
1118 This was estimated from the data sets for the pure and mixed composition scenarios (as in  
1119 the case of  $\Lambda_{\mu}$ ). It resulted that this source of uncertainty has a contribution from  $-8\%$  to  
1120  $+12\%$  to the total MC error depending of the hadronic interaction model.

## 1121 References

- 1122 [1] S. Ostapchenko, Czech. J. Phys. 56 (2006) A149.  
1123 [2] T. Pierog, R. Engel, D. Heck, Czech. J. Phys. 56 (2006) A161.  
1124 [3] W.D. Apel et al. (KASCADE-Grande Collaboration), Astrop. Phys. 24 (2005) 1.  
1125 [4] L. Cazon, R.A. Vazquez, A.A. Watson, E. Zas, Astrop. Phys. 21 (2004) 71; L. Cazon, R.A. Vazquez,  
1126 E. Zas, Astrop. Phys. 23 (2005) 393.  
1127 [5] C. Meurer, J. Bluemer, R. Engel, A. Haungs, M. Roth, Czech. J. Phys. 56 (2006) A211.  
1128 [6] A. Aab et al. (Pierre Auger Coll.) Phys. Rev. D 90 (2014) 012012, erratum: Phys. Rev. D 92 (2015)  
1129 019903(E).  
1130 [7] A. Aab et al. (Pierre Auger Coll.) Phys. Rev. D 91 (2015) 032003, erratum: Phys. Rev. D 91 (2015)  
1131 059901.  
1132 [8] S. Ostapchenko, Nucl. Phys. B (Proc. Suppl.) 151 (2006) 143; S. Ostapchenko, Phys. Rev. D 74 (2006)  
1133 014026.  
1134 [9] E.J. Ahn et al., Phys. Rev D 80 (2009) 094003.  
1135 [10] T. Pierog et al., Phys. Rev. C 92, (2015) 034906.  
1136 [11] S. Ostapchenko, Phys. Rev. D 83 (2011) 014018.  
1137 [12] J. Hersil et al., Phys. Rev. Lett. 6 (1961) 22; D. M. Edge et al., J. Phys. A 6 (1973) 1612.  
1138 [13] W.D. Apel et al. (KASCADE-Grande Collaboration), NIM A 620 (2010) 202.  
1139 [14] K. Kamata, J. Nishimura, Prog. Theor. Phys. Suppl. 6 (1958) 93; K. Greisen in: J. G. Wilson (Ed.),  
1140 Progress in Cosmic Ray Physics, Vol. III, North3 Holland Publishing Co., 1956.  
1141 [15] A.A. Lagutin and R.I. Raikin, Nucl. Phys. B (Proc. Suppl.) 97 (2001) 274.

- 1142 [16] D. Heck et al., Report FZKA 6019, Forschungszentrum Karlsruhe, Germany (1998).
- 1143 [17] Daniel Fuhrmann, *KASCADE-Grande measurements of energy spectra for elemental groups of cosmic*  
1144 *rays*, Ph.D. thesis, University of Wuppertal, Germany (2012).
- 1145 [18] A. Fassò et al., Report CERN-2005-10, INFN/TC-05/11, SLAC-R-773 (2005).
- 1146 [19] R. Brun, F. Carminati, GEANT-detector description and simulation tool, CERN Program Library  
1147 Long Writeup, 1993.
- 1148 [20] W.D. Apel et al. (KASCADE-Grande Collaboration), Phys. Rev. D 87 (2013) 081101(R).
- 1149 [21] W.D. Apel et al. (KASCADE-Grande Collaboration), Astrop. Phys. 36 (2012) 183.
- 1150 [22] S. Ostapchenko, EPJ Web of Conferences 52 (2013) 02001.
- 1151 [23] T. Pierog and D. Heck, Proc. 33rd ICRC, Rio de Janeiro, Brazil (2013) #icrc163; T. Pierog, J. Phys.:  
1152 Conf. Ser. 409 (2013) 012008.
- 1153 [24] P. K. F. Grieder, Extensive air showers: High energy phenomena and astrophysical aspects, a tutorial,  
1154 reference manual and data book, Vol. I, Springer, 2011 edition.
- 1155 [25] W.D. Apel et al. (KASCADE-Grande Collaboration), Phys. Rev. D 80 (2009) 022002.
- 1156 [26] M. Honda et al., Phys. Rev. Lett. 70 (1993) 525.
- 1157 [27] C.J. Bell et al., J. Phys. A: Math., Nucl. Gen. 7 (1974) 990.
- 1158 [28] M. Ave et al., Proc. 27th ICRC, Hamburg, Germany (2001) 381.
- 1159 [29] F. Riehn, R. Engel, A. Fedynitch, T. K.Gaisser and T. Stanev, Proc. 34rd ICRC, The Hague, Nether-  
1160 lands, Proceedings of Science, PoS (ICRC2015) 558.
- 1161 [30] L. Cazon et al., Astropart. Phys. 36 (2012) 211.
- 1162 [31] W.D. Apel et al. (KASCADE-Grande Collaboration), Phys. Rev. D 80 (2012) 022002; J.R. Hörandel,  
1163 J. Phys. G: Nucl. Part. Phys. 29 (2003) 2439.
- 1164 [32] W.D. Apel et al. (KASCADE-Grande Collaboration), Astrop. Phys. 34 (2011) 476.
- 1165 [33] P. Luczak et al. (KASCADE-Grande Collaboration), Proc. 34rd ICRC, The Hague, Netherlands, Pro-  
1166 ceedings of Science, PoS (ICRC2015) 386.
- 1167 [34] T. Antoni et al. (KASCADE Collaboration), NIM A 513 (2003) 490.
- 1168 [35] J. Zabierowski et al. (KASCADE-Grande Collaboration), Proc. 29th ICRC, Pune, India, Vol. 6 (2005)  
1169 357.
- 1170 [36] H.J. Drescher and G.R. Farrar, Astrop. Phys. 19 (2003) 235.
- 1171 [37] R. Engel, Rapporteur talk: Particle and interaction physics, Proc. 27th ICRC, Hamburg, Germany  
1172 (2001) 181.
- 1173 [38] A. Haungs et al. (KASCADE Coll.), The primary energy spectrum of cosmic rays obtained by muon  
1174 density measurements at KASCADE, Proc. 27th ICRC, Hamburg, Germany (2001) 63.
- 1175 [39] A. V. Glushkov et al. (Yakutsk EAS Array Coll.), JETP Lett. 87 (2008) 190.
- 1176 [40] A. Yushkov et al. (Pierre Auger Coll.), Eur. Phys. J. Web. Conf. 53 (2013) 07002; L. Nellen et al.  
1177 (Pierre Auger Coll.), J. Phys.: Conf. Ser. 409 (2013) 012107.
- 1178 [41] T. Abu-Zayyad et al., Phys. Rev. Lett. 84 (2000) 4276.
- 1179 [42] Yu. A. Fomin et al., <arXiv: 1609.05764 [astro-ph.HE]>.
- 1180 [43] J. G. Gonzalez et al. (IceCube Coll.), J. Phys.: Conf. Ser. 718 (2016) 052017.
- 1181 [44] W.D. Apel et al. (KASCADE-Grande Collaboration), J. Phys. G: Nucl. Part. Phys. 36 (2009) 035201.
- 1182 [45] W.R. Nelson, H. Hirayama and D.W.O. Rogers, Report SLAC (1985) 265.
- 1183 [46] G. Antchev et al. (TOTEM Coll.), Europhys. Lett. 96 (2011) 21002; 101 (2013) 21002; 101 (2013)  
1184 21003; 101 (2013) 21004; Phys. Rev. Lett. 111 (2013) 012001.
- 1185 [47] G. Aad et al. (ATLAS Coll.), Nucl. Phys. B889 (2014) 486; M. Aaboud et al. (ATLAS Coll.), Phys.  
1186 Lett. B 761 (2016) 158.
- 1187 [48] T. Antoni et al., Astrop. Phys. 19 (2003) 703.
- 1188 [49] T. Pierog et al., Proc. 34rd ICRC, The Hague, Netherlands, Proceedings of Science, PoS (ICRC2015)  
1189 337.
- 1190 [50] S. Ostapchenko, Phys. Rev. D 93 (2016) 051501(R).
- 1191 [51] T. Pierog et al., Report FZKA 7516, Forschungszentrum Karlsruhe, Germany (2009) 133.
- 1192 [52] J. Allen et al., EPJ Web of Conferences 53 (2013) 01007.

- 1193 [53] R. Ulrich et al., Phys. Rev. D 83 (2011) 054026.  
1194 [54] Alexander E. Hervé for the NA61/SHINE Collaboration, Proc. 34rd ICRC, The Hague, Netherlands,  
1195 Proceedings of Science, PoS (ICRC2015) 330.  
1196 [55] G. Zech, Comparing Statistical Data to Monte Carlo Simulation - Parameter Fitting and Unfolding,  
1197 DESY 95-113 (1995); G. Bohm, G. Zech, NIMA 691 (2012) 171.  
1198 [56] W.D. Apel et al. (KASCADE-Grande Collaboration), Phys. Rev. Lett. 107 (2011) 171104.  
1199 [57] W.D. Apel et al. (KASCADE-Grande Collaboration), Astrop. Phys. 47 (2013) 54.  
1200 [58] V. de Souza et al. (KASCADE-Grande Collaboration), Proc. 32nd ICRC, Beijing, China, Vol. 1/11  
1201 (2011) 295.